ELEMENTAL DISTRIBUTION IN STRIATED MUSCLE AND THE EFFECTS OF HYPERTONICITY

Electron Probe Analysis of Cryo Sections

AVRIL V. SOMLYO, HENRY SHUMAN, and ANDREW P. SOMLYO

From the Pennsylvania Muscle Institute, University of Pennsylvania, Philadelphia, Pennsylvania 19104

ABSTRACT

A method of rapid freezing in supercooled Freon 22 (monochlorodifluoromethane) followed by cryoultramicrotomy is described and shown to yield ultrathin sections in which both the cellular ultrastructure and the distribution of diffusible ions across the cell membrane are preserved and intracellular compartmentalization of diffusible ions can be quantitated. Quantitative electron probe analysis (Shuman, H., A. V. Somlyo, and A. P. Somlyo. 1976. *Ultramicros.* **1**:317–339.) of freeze-dried ultrathin cryo sections was found to provide a valid measure of the composition of cells and cellular organelles and was used to determine the ionic composition of the *in situ* terminal cisternae of the sarcoplasmic reticulum (SR), the distribution of Cl in skeletal muscle, and the effects of hypertonic solutions on the subcellular composition of striated muscle.

There was no evidence of sequestered Cl in the terminal cisternae of resting muscles, although calcium (66 mmol/kg dry wt ± 4.6 SE) was detected. The values of $[Cl]_i$ determined with small (50–100 nm) diameter probes over cytoplasm excluding organelles and over nuclei or terminal cisternae were not significantly different. Mitochondria partially excluded Cl, with a cytoplasmic/mitochondrial Cl ratio of 2.4 ± 0.88 SD.

The elemental concentrations (mmol/kg dry wt ± SD) of muscle fibers measured with 0.5–9-μm diameter electron probes in normal frog striated muscle were: P, 302 ± 4.3; S, 189 ± 2.9; Cl, 24 ± 1.1; K, 404 ± 4.3, and Mg, 39 ± 2.1. It is concluded that: (*a*) in normal muscle the "excess Cl" measured with previous bulk chemical analyses and flux studies is not compartmentalized in the SR or in other cellular organelles, and (*b*) the cytoplasmic Cl in low $[K]_o$ solutions exceeds that predicted by a passive electrochemical distribution.

Hypertonic 2.2 × NaCl, 2.5 × sucrose, or 2.2 × Na isethionate produced: (*a*) swollen vacuoles, frequently paired, adjacent to the Z lines and containing significantly higher than cytoplasmic concentrations of Na and Cl or S (isethionate), but no detectable Ca, and (*b*) granules of Ca, Mg, and P $\simeq$(6 Ca + 1 Mg)/6 P in the longitudinal SR. It is concluded that hypertonicity produces compartmentalized domains of extracellular solutes within the muscle fibers and translocates Ca into the longitudinal tubules.

KEY WORDS electron probe analysis · cryoultramicrotomy · striated muscle · hypertonicity · sarcoplasmic reticulum

The distribution of diffusible ions in, respectively, the extracellular space, cytoplasm, and cellular organelles, represents one of the most general problems of cell function. The main techniques available for determining the concentrations of ions in different compartments are the measurement of radio isotope ion fluxes in intact tissues and organelle fractionation. These techniques are, however, subject to the respective uncertainties of the ultrastructural identification of kinetically defined flux compartments and the possible translocation of diffusible elements during cell fractionation. Therefore, a method suitable for determining quantitatively and directly the composition of cells and organelles is of general interest to cell physiology. The first, and possibly most important, requirement of such a method is a tissue preparatory technique that maintains both the in vivo distribution of diffusible elements and a recognizable ultrastructural organization. The second requirement is that of a sufficiently sensitive physical technique for making the necessary measurements. One of the objectives of this work is to demonstrate that energy-dispersive X-ray analysis of freeze-dried cryo sections can satisfy the above requirements.

In the present study we describe a method of rapid freezing in supercooled Freon 22 that quantitatively preserves in freeze-dried cryo sections of muscle both the transmembrane gradients of diffusible ions and the cellular ultrastructure. The cryo sections obtained with this method were suitable for energy-dispersive electron probe analysis in a transmission electron microscope. The results of quantitative electron probe analysis of ultrathin sections, with a method developed in conjunction with this study (83), were compared to the results obtained with independent techniques and shown to be reliable.

We chose striated muscle as the biological system to study in detail, because of the wealth of available information about the elemental composition of this tissue (e.g., cell K, P), on the one hand, and the existence of some unsettled physiological problems amenable to cryoultramicrotomy and quantitative electron probe analysis, on the other. The ultrastructure of muscle in unfixed cryo sections was compared to that in fixed material, to determine whether the triadic gap could be an artifact of fixation. The major biological questions to be dealt with are the ionic composition of the terminal cisternae of the sarcoplasmic reticulum (SR), the distribution of Cl in striated muscle, and the possible existence of an intracellular compartment having an ionic composition similar to that of the extracellular space. Such a compartment has been suggested by previous authors on the basis of ion flux studies (27, 46, 60, 69, 79), the distribution of fluorescent dyes and other markers (34), and the finding of fiber Cl contents exceeding the amounts predicted by passive electrochemical distribution (46). The apparent correspondence between the size of this kinetically defined compartment and the size of the SR (70, 74) led to suggestions (46, 79) that the SR is in ionic communication with the extracellular space. This hypothesis is not in agreement with electrophysiological measurements (49) including measurements of membrane capacitance (28, 33, 36, 50), but received support from studies showing the swelling of the SR in muscles fixed after incubation in hypertonic solutions (15, 16, 53). Therefore, we also examined cryo sections of muscles treated with hypertonic solutions for evidence of compartmentalized extracellular solutes. An incidental observation of some importance to excitation-contraction coupling was the finding of electron-opaque granules consisting of Ca, Mg, and P in the longitudinal SR of the muscles incubated in hypertonic solutions. Preliminary reports of some of these findings have been published (87, 89).

MATERIALS AND METHODS

Tissue Preparation

The extensor longus digitorum IV, the musculi lumbricales of the toe, and small fiber bundles from the semitendinosus of *Rana pipiens* were used. It was necessary to use muscles that were thin (to optimize freezing) and not longer than the diameter of the freezing microtome's chuck. Frogs were fed daily and were free from obvious infection.

The composition of the frog Ringer's solution in mM was; NaCl, 116; $CaCl_2$, 1.2; KCl, 3.0; $NaHCO_3$, 2.0; with a pH of 7.2 and osmolarity of 245 mosmol/kg H_2O; the 2.2 × hypertonic NaCl Ringer's solution had a total of 270 mM NaCl in the frog Ringer's solution. The 2.2 × hypertonic Na isethionate Ringer's was prepared by replacing the NaCl in the hypertonic NaCl Ringer's solution with 270 mM Na isethionate. 2.5 × hypertonic sucrose Ringer's was prepared by adding 1.198 g of solid sucrose to 10 ml of frog Ringer's fluid. Unless otherwise stated, all solutions contained 10^{-6} g/ml tetrodotoxin

(Sigma Chemical Co., St. Louis, Mo.) to prevent activation. Bovine serum albumin 4% (no. 6003, Sigma Chemical Co.) was added during the final 15 min of incubation to minimize the formation of ice crystals in the extracellular space, unless otherwise stated.

Muscles were stretched to 100–130% of slack length, their tendons tied to a stainless steel holder, and incubated in Ringer's solution from 15 to 180 min at room temperature. The muscle was examined under a dissecting microscope for damaged fibers just before freezing. Specimens with damaged fibers were discarded. After preincubation in normal Ringer's, for 15–150 min, some muscles were incubated in hypertonic NaCl, Na isethionate, or sucrose Ringer's solution for 30 min at room temperature. The morphology of and the ion distribution in muscles exposed to hypertonic solutions were similar regardless of the duration of preincubation in normal Ringer's solution, and, therefore, these results are reported together.

A special low mass stainless steel holder (Fig. 1) was designed to hold the whole muscle during freezing and sectioning. The use of cubed tissues (23) was not suitable for the study of muscle, due to the movement of ions through cut surfaces. The configuration of the muscle mounted in the holder was such that there was a very small (~1 mm^2) dome of muscle presenting a cutting face at the tip that did not require trimming. This dome configuration also assured that no matter how deeply sections were cut, the periphery of the section still included some of the muscle surface that was frozen at the fastest rate.

Tissue Freezing and Cryoultramicrotomy

The techniques previously used for cryoultramicrotomy (4, 5, 10, 23) required some further modifications for the present study. It was obviously necessary to avoid the use of stabilizing agents such as glutaraldehyde and cryoprotectants such as glycerol or dimethylsulfoxide, and to analyze only sections picked up from the dry knife without floating them on a liquid surface that would permit the diffusion of ions.

After incubation, the holders were carefully blotted with filter paper. The muscles were blotted at the tendon regions only. The holder, with the muscle cutting face downward, was quickly clipped into the silver wire of the freezing apparatus (Fig. 2), swung over the container of coolant and fired into 100 ml of supercooled Freon 22 (monochlorodifluoromethane) with an air gun operated at a velocity of 60 cm/s. The time from removal from the Ringer's to freezing was ~15 s. The Freon 22 was vigorously stirred with a magnetic stirrer and cooled in a styrofoam container of liquid nitrogen. The temperature was monitored with a thermistor and tissues were frozen at -164 ± 2°C, above the solidification temperature of -175°C. Upon solidification of the Freon 22 the temperature rose to the normal freezing point of -160°C. Vigorous stirring is required for supercooling Freon (a chance observation) and for maintaining a uniform temperature in the coolant. The supercooled Freon 22 was found to yield superior freezing to a liquid N_2 slush produced by cooling liquid N_2 through vacuum pumping a surrounding container of liquid N_2 (boiling point, -196°C; freezing point, -210°C), as judged by the number of ice crystal-free sections obtained. Preservation of ice crystal-free structures at the electron microscope level requires freezing rates of >5,000°–10,000°C/s. (5, 19, 23, 42, 71, 77).

The LKB cryoultramicrotome (LKB Produkter, Bromma, Sweden) was modified so that the ambient temperature in the cryo chamber was -130°C. A similar modification was reported while this work was in progress (30). The liquid N_2 normally pumped into the knife holder was directed into a large foil trough of about 7 × 3 inches at one end of the chamber. The entire chamber was insulated with styrofoam. The knife was maintained at -100°C and the specimen at -110°C. Glass knives were used for the majority of the experiments, and a fresh area of the knife edge had to be used about every five sections because the knives became dull very quickly when cutting frozen tissues. Diamond knives were used occasionally and it is our impression that they are more suitable for cutting thinner sections. Section thickness was difficult to control due to minor instabilities of the advance mechanism of the microtome, and ranged from

FIGURE 1 Low-mass stainless-steel-mesh muscle holder shown with a toe muscle mounted. In 1*a*, the holder is mounted in the microtome chuck. The portion of the muscle (dotted line) on the top of the domed holder, as seen in the side view of Fig. 1*b*, serves as the cutting face.

FIGURE 2 Freezing apparatus. The air gun *A* operated at 80 lbs/$inch^2$ shoots the muscle and stainless-steel mesh holder, clipped to the silver wire (arrow) into the Freon 22. *N*, compressed gas line. *S*, solenoid. *F*, styrofoam cup holding a beaker with 100 ml of Freon 22 immersed in liquid N_2. *M*, magnetic stirrer. Double arrow, thermistor immersed in Freon 22.

FIGURE 3 Frozen-dried section of unfixed normal frog toe muscle showing *A* band, *I* band, *Z*, and *M* lines. Note knife marks and fine compression lines at right angles to the knife marks. Unstained. Bar, 1 μm. × 22,500.

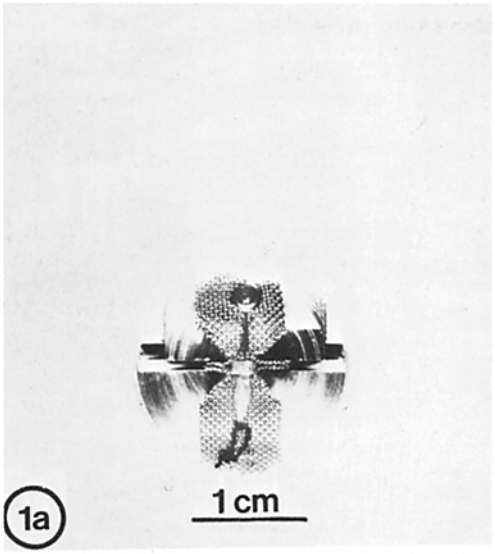

1a

1b

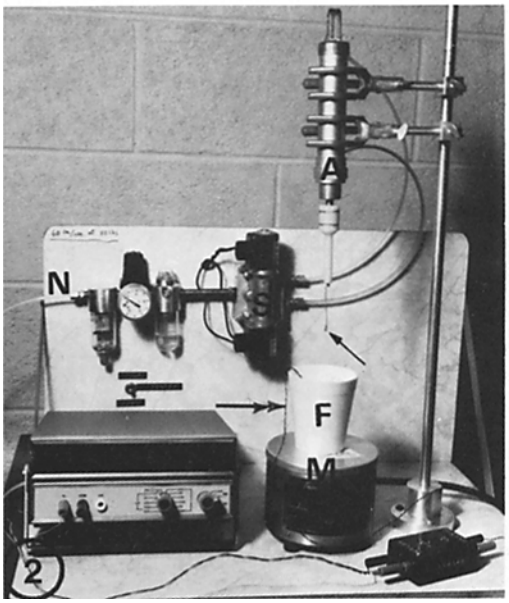

2

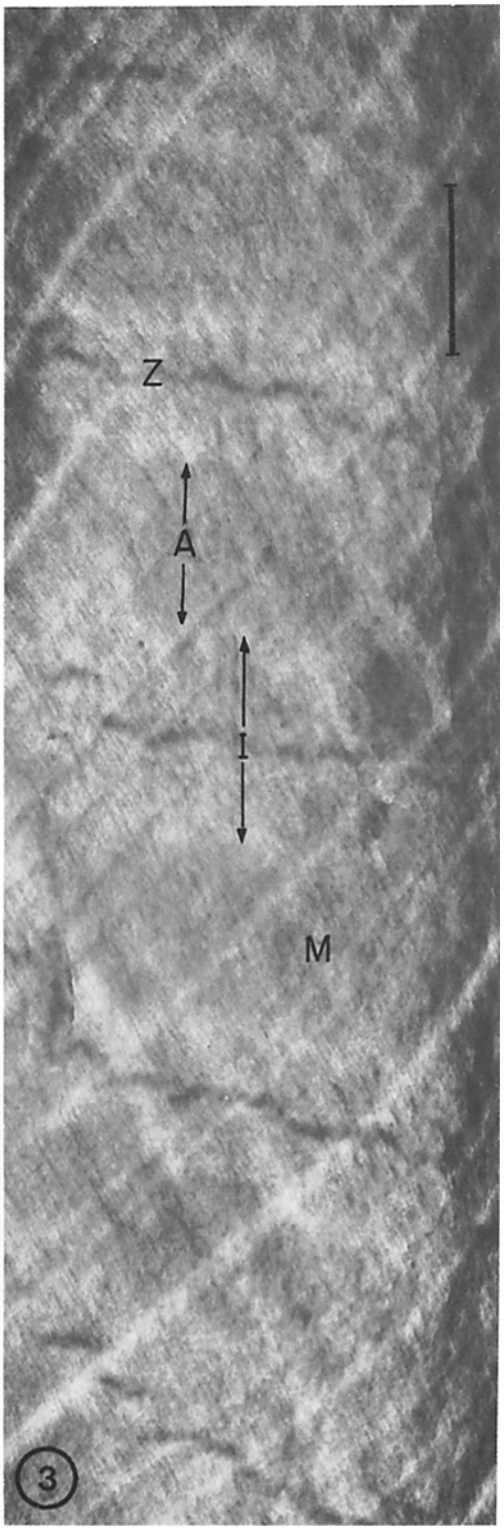

3

900 to 2,000 Å as judged by the gray-to-blue interference colors. The thinner, more electron-lucent sections were used for imaging and analyzing terminal cisternae. The dry sections were picked up with chilled orange stick splinters from the knife edge through the opening on the top of the cryokit and placed on the grids. Copper grids were held on a small silver tray molded to fit over the knife holder. Carbon-coated Formvar films on copper or nylon grids were used in the earlier part of this study, but the image resolution of the sections was much improved in later experiments with the use of carbon support films, prepared by evaporating carbon onto freshly-split mica, floating the carbon film onto a water surface, and subsequently submerging the Cu grid and picking up the C film. After drying, the grids with carbon films were glow-discharged. The sections were sandwiched between two of the carbon film-covered copper grids and stamped with a liquid N_2-chilled, polished brass rod. Breaks in the film were common, possibly caused by the stamping. These breaks frequently exposed sufficiently large areas of muscle suitable for analysis without an underlying film, but still stable under the beam. The silver tray with the grids was transferred to a liquid N_2-chilled brass cup covered with a heavy brass lid and transported in liquid N_2 to the Denton vacuum evaporator (Denton Vacuum Inc., Cherry Hill, N. J.) where the grids were frozen-dried by pumping at 10^{-5}–10^{-7} Torr overnight. Within 25 min the temperature of the brass cup was −80°C and the vacuum was 5.5×10^{-6} Torr. The saturation vapor pressure of ice at −80°C is $\sim 1 \times 10^{-4}$ Torr, and ice sublimation from a 100-nm section occurs in about 10 s (78). Grids were carbon-coated and stored in a desiccator. One grid from each experiment was stained with osmium vapor *in vacuo* for 10 min to enhance contrast.

Electron Probe X-Ray Analysis

The principles of electron probe analysis have been discussed in detail by Hall (45), and several biological applications of the method have been reported (5, 24–26, 29, 41, 44, 54, 64, 65, 76, 88, 90, 91).

We used a Philips EM 301 transmission electron microscope having a goniometer stage modified to accept a 30 mm^2 (20° specimen-to-detector angle, 0.067 steradians solid angle, 160 eV resolution) Kevex Si(Li) X-ray detector (Kevex Corp., Burlingame, Calif.) interfaced with a Kevex 5100 multichannel analyzer and a Tracor Northern NS 880 computer and TN 1000 magnetic tape recorder (Tracor Northern, Middleton, Wis.). A modified Philips liquid nitrogen-cooled holder, operated at −100° to −110°C, was used to minimize contamination and mass loss. The detailed characteristics of the system have been described previously (83).

The X-ray spectrum obtained in a transmission electron optical column from a thin section includes the characteristic peaks due to elements $Z \geq 11$ present in the specimen and the associated continuum largely arising from the organic matrix. It also contains instrumental peaks (the largest one being the Cu signal K_α = 8.047 keV) from the specimen grid and holder, with an associated extraneous continuum, and low-energy noise probably due to electrons reaching the detector. These extraneous signals and the associated continuum can be measured by collecting the spectrum generated with the beam passing through an empty grid hole, and are subtracted by the computer routine as is the low-energy noise level (83). The presence of a variable, but frequently large, Si peak can be due to contamination from pump oils and vacuum seals used in the electron microscope and vacuum evaporator, and signal originating from the dead layer of the detector. Therefore, no inference should be drawn regarding the biological occurrence of silicon from the present study.

The measurement of elemental concentrations is based on the fact, pointed out by Hall (45), that for elements of atomic number $Z \geq 11$–20 in concentrations of <1 M/kg, the characteristic peak/X-ray continuum ratio is linearly related to the concentration/dry mass ratio. The peak counts in the unknown peak and its error of measurement are computed together with the counts in a continuum band (1.34–1.64 keV) that has the smallest relative error in specimens that do not contain aluminum (in view of the Al K lines at 1.3–1.5 keV). The peak/continuum ratio is obtained and is converted to an elemental concentration by using a proportionality constant obtained from linear calibration curves of standards.

The basic equation for quantitation is:

$$C_x = \frac{I_x}{I_b} \times W_x,$$

where C_x is the concentration of element x, I_x is the number of characteristic peak counts for that element, I_b is the number of continuum counts, and W_x is a quantitation parameter relating concentration to peak/background ratio and is obtained from standards. W_x includes the effects of ionization cross sections, fluorescence yield, and detector efficiency for each specific element. As an example, the ratio of the characteristic potassium peak to the continuum counts I_K/I_b in the center panel of Fig. 17 is 12,359/2,631 = 4.6957 and W_K is 105.7 (83); therefore, the K concentration (C_K) is 496 mM/kg dry wt. A detailed description and validation of quantitative electron probe analysis of thin sections, with an accuracy of ~10%, has been published elsewhere (83, 84).

The minimal detectable concentration of potassium, with our instrumentation, is 10 mM/kg dry wt in a 100-nm section during a 100-s count at 1,000 cps (83, 84). The minimal detectable concentration of Cl is similar to that of K; however, the detectability of Na is worse by a factor of ~5.9 (see Discussion). Therefore, the Na concentrations measured with small spots are subject to rather large errors.

The probe currents used ranged from 0.4 nA to 3.5 nA, and the probe diameters from ~50 nm to 14,000 nm. The larger (0.5–1.4 μm) probes were used to determine the "bulk" fiber concentrations reported in Tables

I, II, and IV. For comparison of terminal cisternae and mitochondria with the adjacent cytoplasmic regions, paired analyses were done in every case with identical probe parameters (current, spot diameter, and analysis time). Small probes (~50–200 nm, sufficient only to cover the organelle analyzed) were used for this purpose. This procedure allowed a comparison of the absolute number of counts in a given peak (proportional to the mass of that element in the volume analyzed) in addition to the concentrations measured through the characteristic peak/X-ray continuum ratio. The contents of the broken vacuoles or "holes" (see Results) were analyzed by placing (50–100 nm) probes on the edges or the strands running across the holes. All small spot analyses were done at −100°C to avoid contamination that would contribute to the X-ray continuum. The cold holder drifts about 10 Å/s, thus, with small spot analysis at low temperature it was necessary to interrupt the analysis every 25–50 s to check the position of the structure under analysis. Spectra from four to six 100-s counts over terminal cisternae or cytoplasm were summed. This approach also allowed us to reduce the radiation dose delivered with small probes to ~500 coulomb/cm². The dose delivered with a 4-μm probe in 300 s is ~15 coulomb/cm². Both values are within the range tolerated with <15% mass loss (83, 84).

Osmium vapor staining *in vacuo* of frozen-dried sections contributes substantially to the X-ray continuum as well as giving the characteristic osmium lines. Because the presence of osmium increases the error in quantitation (83), unstained sections were used for all the quantitative analyses. Electron micrographs of osmium vapor-stained sections are used for optimal illustration of morphology. Occasionally, qualitative analyses were done on osmium-stained material.

Statistical Treatment of the Data

Variations of elemental concentration in biological material as measured by quantitative energy dispersive X-ray analysis are due to two sources: real cell-to-cell or intracellular variations and random fluctuations in X-ray production and detection, as determined by poisson statistics. Since the statistical properties of energy dispersive analysis are known, the two types of variations can be, to some extent, identified (83).

For each individual measurement (each spectrum) the random error of peak counts and continuum counts can be estimated. The concentrations in Tables I and V are shown with the individual standard deviations, predicted from these random errors. Because the peaks are normally superimposed on a statistically noisy background, it is possible to have a nonzero standard deviation even when that element is absent from the specimen. It is also possible for the noisy background to make it appear as though a small negative peak were present. The negative concentrations do not have biological significance.

In analyses of regions that have very little dry mass, such as areas of the extracellular space devoid of connective tissues, it is possible to have large standard deviations (e.g., 50%) of the concentrations even though the elemental peaks are very large and accurately measured. In this case, the relatively large standard deviation of the concentration is due to the low number of counts in the continuum region with its large relative error. Therefore, the certainty of the element being present is much greater than the certainty of its concentration. When comparing extracellular spaces that generate low continuum counts or two areas that may have had very different degrees of hydration, it is useful to compare the actual peak counts (using identical probe parameters and counting times) as well as the concentrations. This was done in the present study for the paired analyses of mitochondria-adjacent cytoplasm, nuclei-cytoplasm, and vacuoles-cytoplasm.

The standard deviations of the individual measurements can be improved by increasing the number of counts in a given peak. This is accomplished by increasing the counting time, increasing the probe current in the microvolume analyzed, or increasing the absolute amount of elements (such as by increasing section thickness) in the volume irradiated.

Because the precision of the individual concentration measurements varies, mainly due to differences in specimen thickness and counting time, the average concentration over different fibers must be a weighted average (11). The weighted mean μ is given by:

$$\mu = \frac{\Sigma(x_i/\sigma_i^2)}{\Sigma 1/\sigma_i^2}, \tag{1}$$

where x_i is the concentration (or peak counts), and σ_i^2 is the predicted variance of each measurement.

The standard error of the mean (SEM) and the standard deviation of the fit S(SD) are the square roots of the respective variances σ_μ^2 and S^2 (11).

The χ^2 value is used to determine whether fiber-to-fiber (or muscle-to-muscle) variations could be explained on the basis of measurement errors. The "chi-squared" test compares the variance of the mean, σ_μ^2, to the variance of the fit, S^2, where

$$\sigma_\mu^2 = 1/\Sigma\,(1/\sigma_i^2). \tag{2}$$

The χ^2 is defined to be:

$$\chi^2 = \Sigma(\chi_i - \mu)^2/\sigma_i^2, \tag{3}$$

and the reduced χ_ν^2 is given by

$$\chi_\nu^2 = \frac{\chi^2}{\nu} = \frac{S^2}{N\sigma_\mu^2}, \tag{4}$$

where $\nu = N$-1, the number of degrees of freedom, N is the number of measurements (11). If $\chi_\nu^2 = 1$, then the variations in the measurements are entirely due to random errors.

The probability values P shown in Table II give the probability that a random sample of elemental concen-

trations would yield a value of χ^2 as large as or larger than that observed if the parent distribution were equal to the assumed distribution. A small P value, therefore, suggests variations greater than those that can be accounted for by errors in measurement.

RESULTS

Morphology of Normal Muscle

Whole sections free of ice crystal damage at magnifications of about 20,000 could be obtained with our freezing method to a tissue depth of about 5-10 μm. At greater depths the section had a "vitreous" periphery with ice crystals of increasing size appearing towards the center of the section. Vitreous freezing generally permitted better visualization of the fine structure at high resolution, although the contrast of the sarcomere pattern was enhanced in some sections showing fine (~50-100 Å) ice crystal formation. A bands, I bands, and Z and M lines were well defined in unstained sections (Figs. 3, 4, and 18). Fine compression lines at right angles to the knife marks were frequently present (Fig. 3). The presence of knife marks on the frozen-dried sections (Figs. 3, 4, and 11) indicated that it was unlikely that any melting had taken place during the procedures after sectioning. There was sufficient mass contrast even in some of the unstained sections to discern fine structure, and occasionally mitochondrial cristae could be visualized. Exposure of the sections to osmium vapor *in vacuo* naturally enhanced the contrast of membranes and filaments.

The junctional gap, traversed by periodic foot processes, between the junctional T tubule and the junctional SR has been described in fixed material (38, 74) similar to that shown in Fig. 5. The junctional gap in unfixed cryo sections prepared without cryoprotectants is illustrated in Figs. 6–8. The T tubule has a flattened oval shape in cross section (Fig. 8), similar to that found in fixed sections, and there is a junctional gap that in cryo sections measures 8-14 nm. In the unfixed material, as shown in Fig. 6, periodic structures suggestive of foot processes can also be seen. Examples of osmium-stained terminal cisternae and longitudinal SR including the fenestrated collar are illustrated in Figs. 9 and 10.

Morphology of Muscles Incubated in Hypertonic Solutions

The proportion of sections free of ice crystal damage was greater in muscles that were incubated in hypertonic solutions than in normal muscles, because of the reduction in cell water content by hypertonicity.

In muscles incubated in hypertonic solutions (NaCl, sucrose, or isethionate), there were oval, membrane-bounded structures adjacent to the Z lines and with their long axis parallel to the fiber axis (Figs. 11 and 14). These structures, heretofore referred to as vacuoles, were frequently paired and were present in locations normally occupied by the terminal cisternae. However, the vacuoles were wider and longer (Fig. 12) than the comma-like terminal cisternae of the normal muscles (Figs. 5 and 6). Some of the vacuoles, paired and unpaired, were broken ("holes") and their contents collapsed on the edge or in strands across the electron-lucent structures. The breaks in the vacuoles were more frequent and larger where a knife mark was running along the Z line. The vacuoles (broken and unbroken) contained NaCl (see the section on Electron Probe Analysis). The membrane surrounding the vacuoles was sometimes adjacent to the longitudinal SR (Fig. 12), but there was no evidence of vacuolation (swelling) of the longitudinal reticulum or of the fenestrated collar.

Muscles incubated in 2.5 × hypertonic sucrose solutions also showed, in addition to the vacuoles along the Z lines (Figs. 13 and 14), a "bubbled" appearance of both the extracellular space and the vacuoles (Figs. 13 and 14). Sucrose is subject to ~50% mass loss under the electron beam (83), and the bubbled appearance is indicative of sucrose in these regions.

Electron-opaque granules were found in the longitudinal (Fig. 16) and the fenestrated SR tubules in every fiber treated with hypertonic NaCl, sucrose, or Na isethionate, and were more frequent in the hypertonic sucrose than in the NaCl solution. The composition of the granules is described below.

Electron Probe Analysis of Normal Muscles

The ionic concentrations measured in 34 fibers from five frogs with probe diameters ranging from 0.5 to 9.0 μm are shown in Table I and summarized in Table II. Each concentration in Table I represents one analysis with its SD. An analysis of variance of the P, S, Cl, K, and Mg concentrations of the 34 fibers shows that the estimated variance of mean concentrations between frogs is significantly larger than the estimated variance within

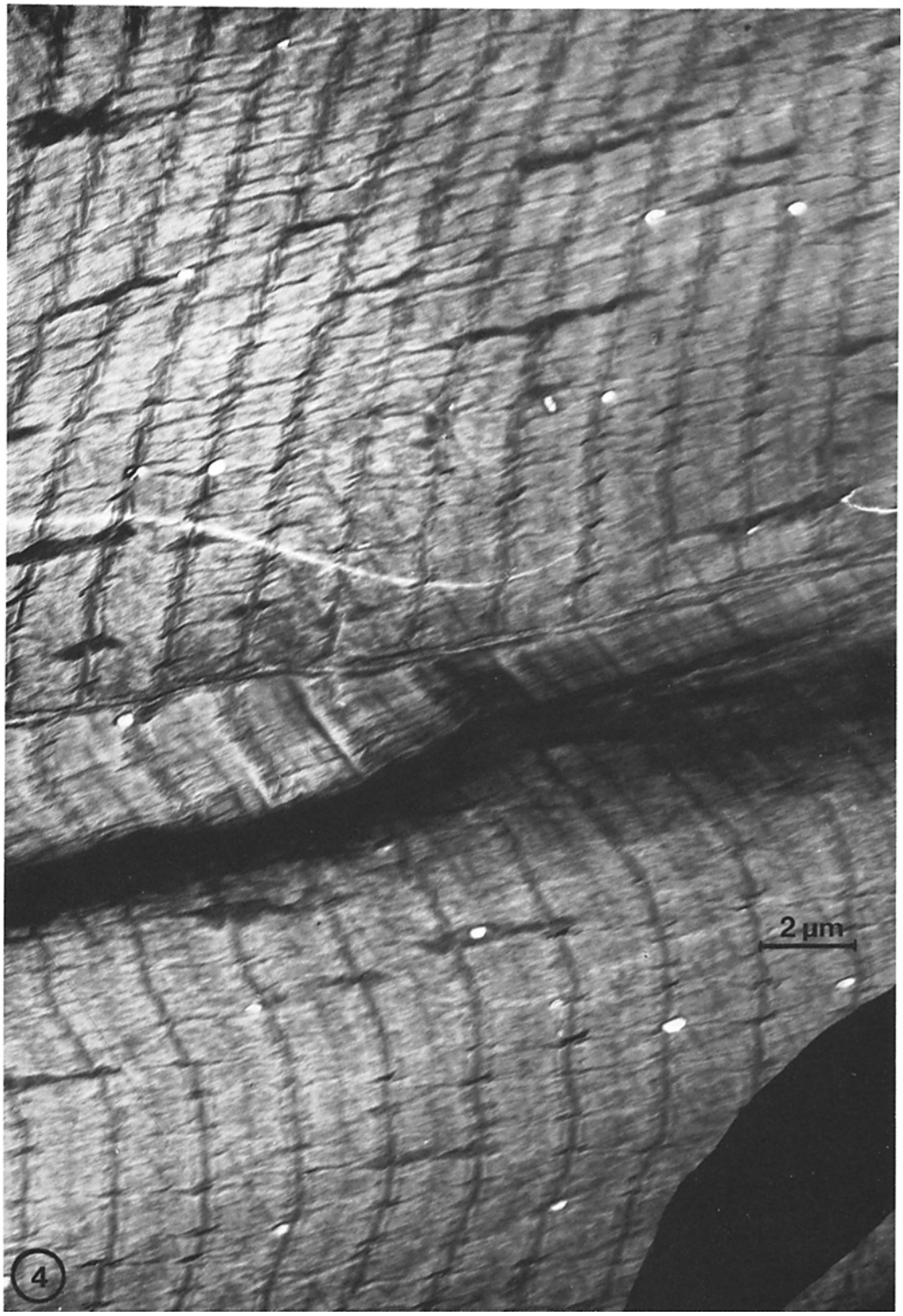

FIGURE 4 Low magnification view of a frozen-dried section of two frog toe muscle fibers. Some regions are out of focus because the section does not lie flat on the grid. Unstained. × 7,500.

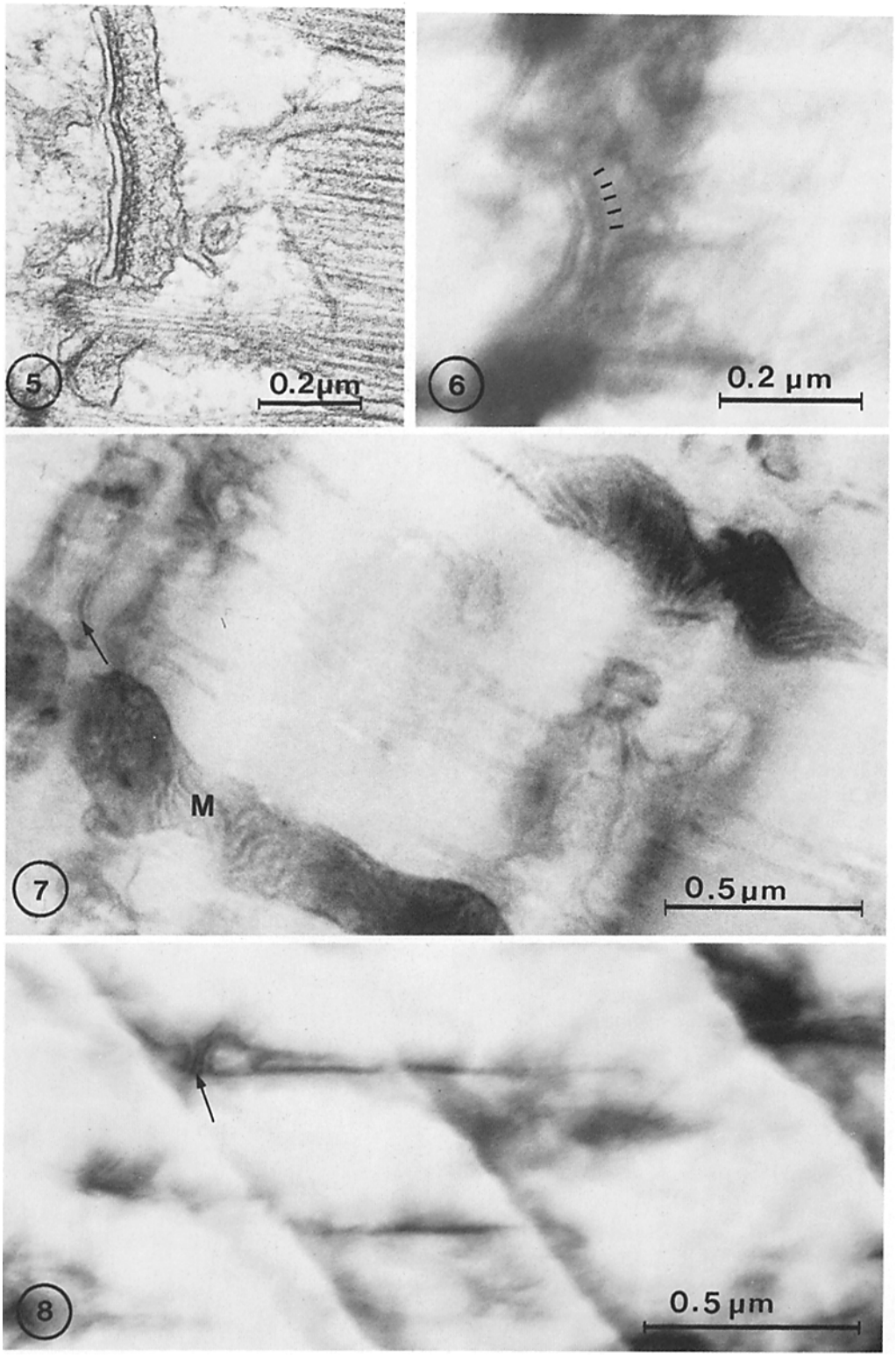
5
0.2μm
6
0.2 μm
M
7
0.5 μm
8
0.5 μm

frogs. The χ_ν^2 values for P, S, Cl, and K concentrations measured in all the muscles give probability values of <0.001, indicating that it is highly unlikely that these differences in ion concentrations measured on a dry weight basis in different frogs were due to the statistical error in measurement. In the case of the Mg, there is a 50% probability that the variations were within the range of measurement statistics.

χ_ν^2 analyses of the fiber elemental concentrations within one muscle, shown in Table II (column 5), in general have high P values, indicating that the variations in elemental concentrations in different fibers of a single muscle are within the range of measurement statistics. There were three exceptions: the K in frogs B and C and the P in frog C. Fiber 9 from frog C shown in Table I has the lowest K and its P is also the lowest for that frog. The fiber with the highest K (fiber 1) also has the highest P. Fiber 9 has 36% less P and 40% less K than fiber 1. The Cl in these two fibers could also differ by the same magnitude considering their standard deviations, although the P value for the χ_ν^2 of the Cl of frog C is 0.5.

The concentrations measured over different areas of cytoplasm of the same fiber, including analyses done within 500 nm of the cell membrane, were within the limits of variation due to count statistics (Fig. 17). Analysis of the extracellular space within 500 nm of a fiber showed no indication of K "spilled" from the fiber. These very sharp boundaries of ions across the cell membranes indicate that the normal ion distribution was preserved by the freezing techniques. Sharp ionic gradients across membranes at 100 nm spatial resolution are also demonstrated in Table V and Fig. 15 from a muscle exposed to hypertonic sucrose (to be discussed later).

In muscles incubated in normal Ringer's solution, analyses of fourteen mitochondria (from six frogs) showed no evidence of Cl accumulation in these organelles. The K/Cl ratios obtained in paired analyses over mitochondria and adjacent cytoplasm were, respectively, 20.2 and 11.7; $P < 0.001$. The K cytoplasm/K mitochondria ratio was 1.4 ± 0.4 SD and the Cl cytoplasm/Cl mitochondria ratio was 2.4 ± 0.8 SD. Because the values expressed as concentrations are based on dry weight and because the relative dry masses of the mitochondria and cytoplasm differ, the data were also evaluated in terms of the total number of characteristic counts collected in paired analyses, using identical probe parameters, with the following results: the ratio of K counts cytoplasm/K counts mitochondria = 1.0 ± 0.3 SD, and the ratio of Cl counts cytoplasm/Cl counts mitochondria = 1.9 ± 0.7 SD. These results indicate a relative exclusion of Cl by the mitochondria. The ratio of mitochondrial phosphorus to cytoplasmic phosphorus was always >1.

The mean ratio of K counts cytoplasm/K counts in five nuclei (from five frogs) was 0.9 ± 0.2 SD. The ratio of Cl counts cytoplasm/Cl counts nuclei was 1.4 ± 0.5 SD, thus also ruling out the nuclei as sites of Cl compartmentalization. While the mean Na concentrations/dry wt did not differ over the cytoplasm, mitochondria and nuclei, the standard deviations for Na were up to 50 mmol/kg dry wt.

Paired analyses of terminal cisternae and adjacent cytoplasm are given in Table III, and an example is shown in Fig. 18. Representative spectra are shown in Fig. 19. To minimize inclusion of cytoplasm in the microvolumes of terminal cisternae analyzed, the probe diameters used for the analyses were ~50 nm. The mean Ca concentration detected over the terminal cisternae was 66 mmol/kg dry wt. ± 4.6 SEM. The slightly higher Na and Cl concentrations over the terminal cisternae than over the cytoplasm are within statistical

FIGURE 5 Longitudinal section of frog toe muscle showing terminal cisterna, foot processes, and T tubule. Glutaraldehyde-, osmium-fixed, stained, and embedded. × 75,000.

FIGURE 6 Unfixed frozen-dried section showing T tubule, junctional gap, and foot processes (bars). Osmium vapor stained. × 108,000.

FIGURE 7 Unfixed frozen-dried section showing a "face view" of the T tubule (arrow) with paired terminal cisternae, longitudinal SR, fenestrated collar and mitochondrion (*M*). Note the T tubule-SR gap. Osmium vapor stained. × 60,000.

FIGURE 8 Unfixed frozen-dried thin section of frog toe muscle showing the T tubule (arrow), T tubule-SR gap, and terminal cisterna. × 66,000.

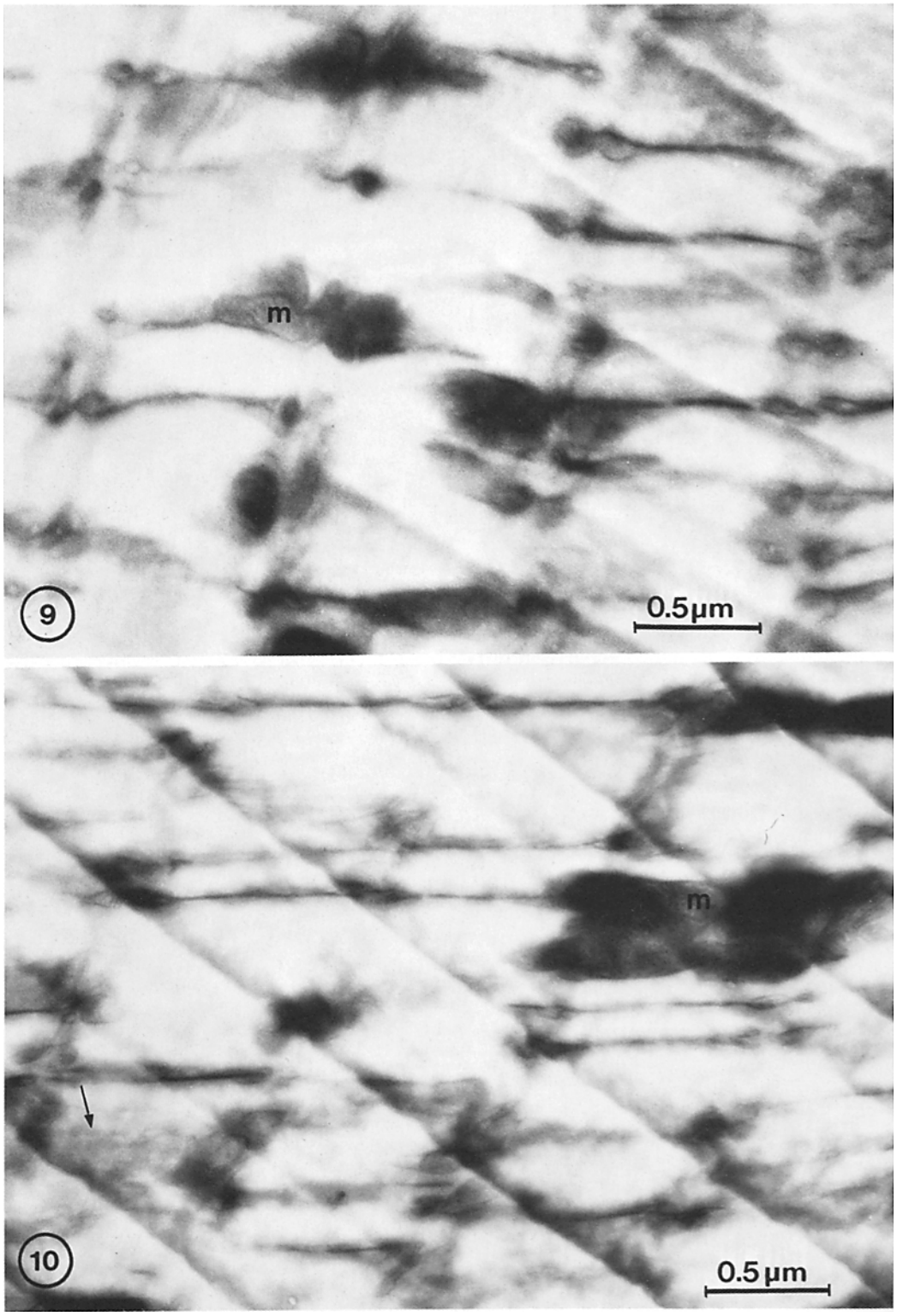

FIGURES 9 and 10 Longitudinal frozen-dried sections of frog toe muscle showing well stained terminal cisternae, mitochondria (*m*), and fenestrated collar (arrow). Osmium vapor stained. × 39,000.

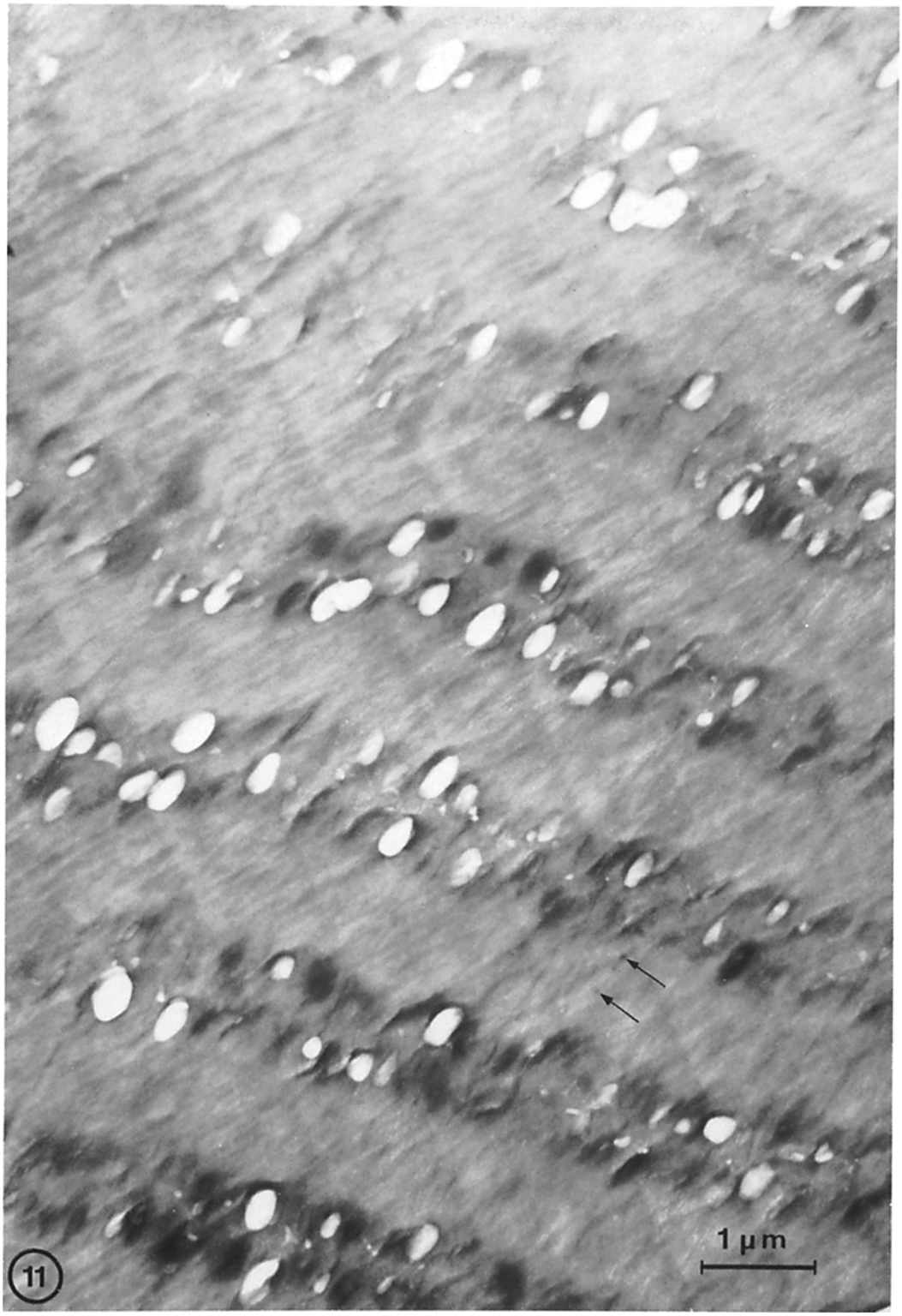

FIGURE 11 Frozen-dried section of frog semitendenosus muscle incubated in 2.2 × hypertonic NaCl solution for 30 min. Frequent paired vacuoles occur along the Z line. Ca granules (arrows) are shown in the longitudinal SR. Osmium vapor stained. × 18,000.

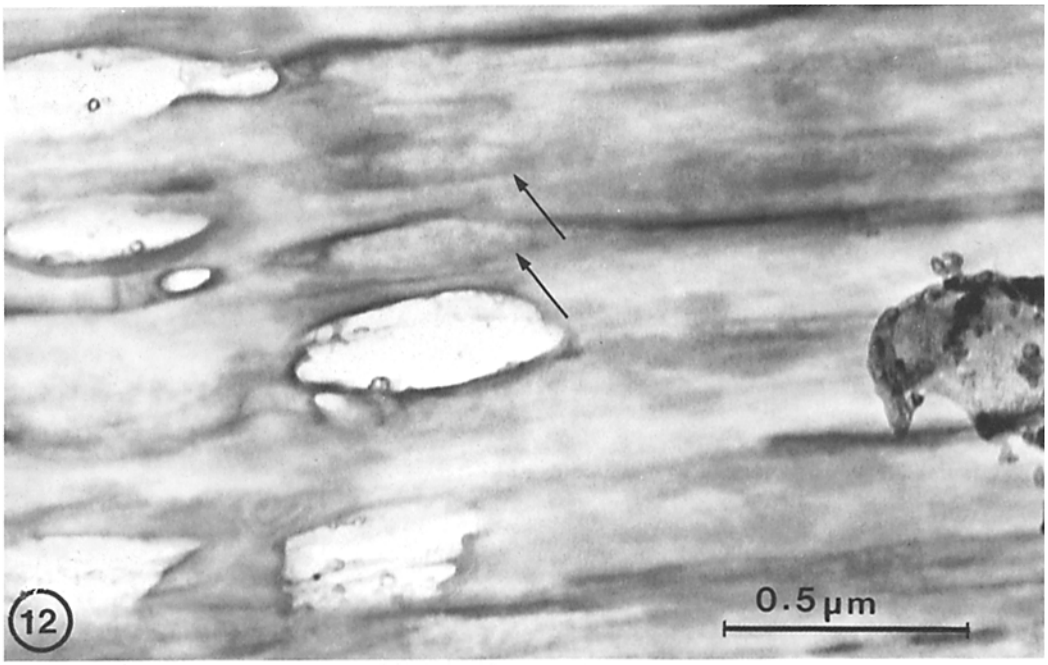

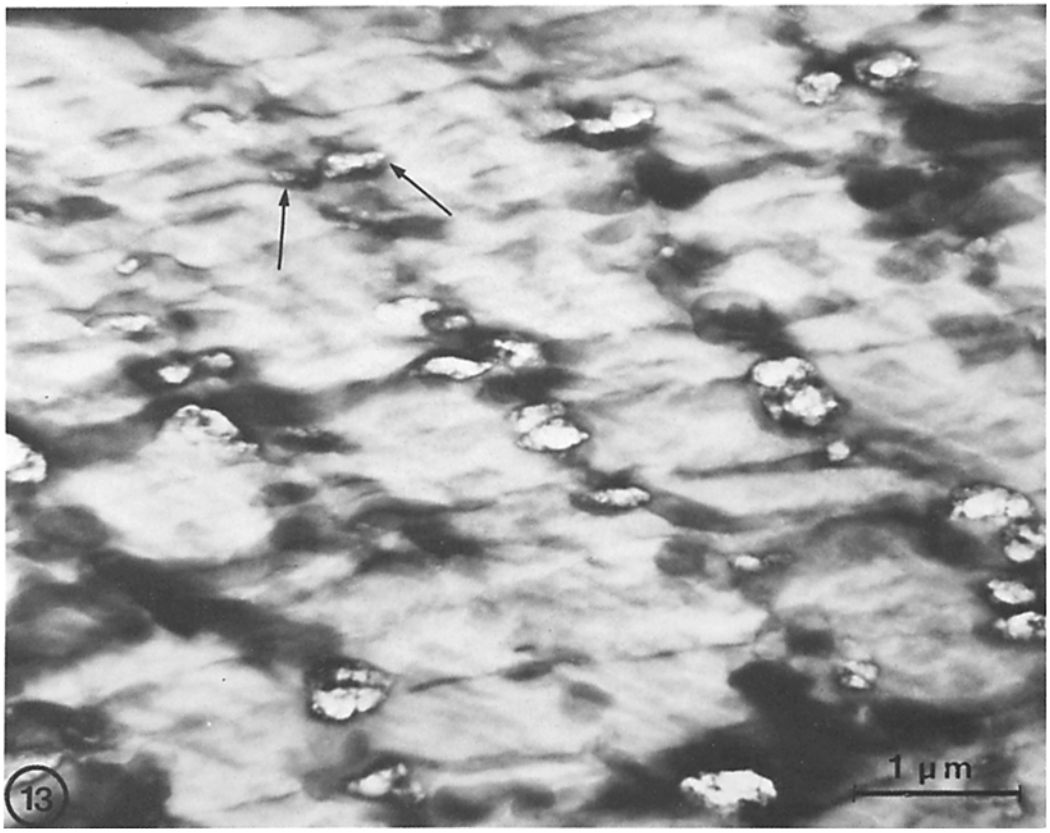

FIGURE 12 High magnification view of swollen (arrows) and vacuolated structures after incubation in 2.2 × hypertonic NaCl solution. Osmium vapor stained. × 66,000.

FIGURE 13 Frozen-dried section of frog toe muscle after incubation in 2.5 × hypertonic sucrose solution. Paired vacuoles indicated by arrows. Osmium vapor stained. × 23,000.

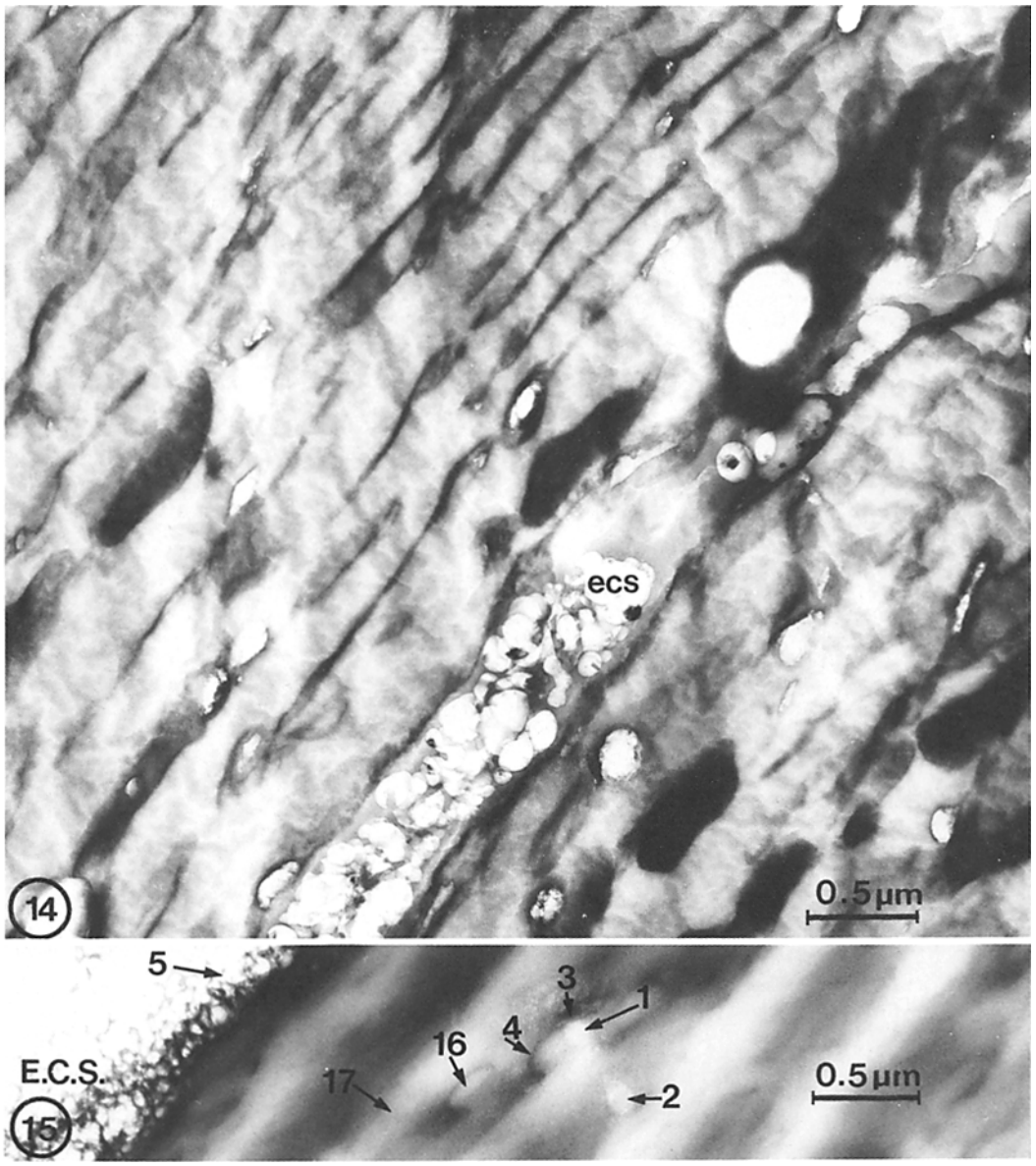

FIGURE 14 Frozen-dried section of frog toe muscle after incubation in 2.5 × hypertonic sucrose solution. Note the typical "bubbled effect" of the sucrose in the extracellular space (*ecs*) and in the oval structures at Z line. × 30,000.

FIGURE 15 A portion of a fiber and adjacent extracellular space (*E.C.S.*) from a frozen-dried section of a frog toe muscle after incubation in 2.5 × hypertonic sucrose solution. The dark bands are due to compression of the section. Areas of analyses are indicated and the elemental concentrations are shown in Table V. The micrograph was taken after analyses nos. 1 and 2, and the areas of mass loss show the location and area analyzed. × 30,000.

error. The phosphorus concentration was higher over the terminal cisternae than over the adjacent cytoplasm. This was probably due to the phospholipid content of the SR membrane, although the possibility of some of the P being associated with Ca cannot be ruled out.

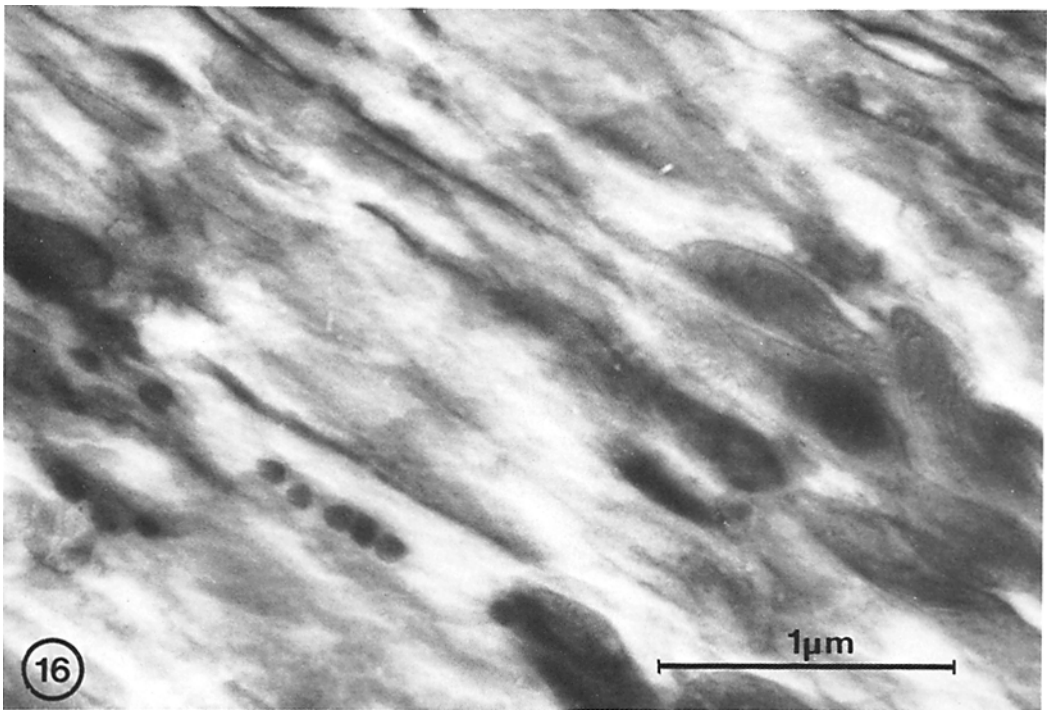

FIGURE 16 High magnification view of a muscle incubated in 2.5 × hypertonic sucrose illustrating the granules occurring in muscles incubated in hypertonic solutions. Osmium vapor stained. × 39,000.

Electron Probe Analysis of Muscles Incubated in Hypertonic 270 mM NaCl Solutions

The results of 60 large-spot (0.5–14 μm diam) analyses of 16 fibers from four toe muscles and one semitendinosus muscle are summarized in Table IV. The variation of cytoplasmic Na and Cl within fibers depended on the number of vacuoles included in the area analyzed. This was most evident where paired vacuoles were seen along the Z lines. For example, analysis of three vacuolated areas and three areas excluding the obvious vacuoles in the same fiber showed K/Cl ratios of, respectively, 6.7, 5.8, and 14.9; and 17.1, 20.0, and 25.0.

In 75 paired small-probe analyses of 14 fibers from five frog muscles incubated in 2.2 × hypertonic NaCl, the K/Cl ratio over the vacuoles (3.7 ± 2.6) was significantly lower ($P < 0.001$) than over the cytoplasm (15.8 ± 5.5). Representative X-ray spectra are shown in Fig. 20.

The marked differences in the K/Cl ratios over the two areas could be due to an increased Cl and/or a decreased K in the vacuoles. The X-ray continuum, representative of dry mass, may also be different in the two regions. For example, if the swollen structures were much more aqueous than the surrounding cytoplasm, the mM/kg dry wt concentrations would be appropriately increased and the comparison of the two regions on the basis of concentrations/dry weight would not be meaningful. These effects can be eliminated by comparing the absolute number of X-ray counts generated in a particular peak for identical counting time, probe size, and current. Under these conditions, the counts obtained are proportional to the absolute amounts of the respective elements contained in the microvolume analyzed. Using this approach in 33 paired analyses over vacuoles and adjacent cytoplasm, the means and SEM for Na[1] and Cl counts over the vacuoles were 657 ± 98 and 1,446 ± 33 and over the cytoplasm they were 334 ± 47, and 384 ± 57 ($P < 0.001$). Thus, the

[1] The Na counts detected are lower by a factor of 5.6 than the Cl counts obtained from an equimolar (NaCl) mixture, due to different absorption in the beryllium window of the Si(Li) detector, the X-ray cross section, and fluorescence yield (83).

TABLE I

Normal Fiber Elemental Concentrations

Frog	Date	Fiber no.	Area analyzed (diam)	P	S	Cl	K	Mg	Na
			μm	*mmol/kg dry wt ± SD*					
A	2/13/76	1	3.0	365 ± 81	152 ± 40	46 ± 20	413 ± 86	68 ± 37	128 ± 82
		2	3.0	312 ± 30	113 ± 14	83 ± 11	383 ± 33	49 ± 16	123 ± 35
		3	3.0	293 ± 30	129 ± 17	42 ± 9	367 ± 33	54 ± 17	97 ± 34
		4	0.5	336 ± 49	148 ± 26	53 ± 15	415 ± 55	33 ± 24	126 ± 58
B	2/9/76	1	3.5	275 ± 19	209 ± 15	18 ± 5	392 ± 23	42 ± 11	44 ± 19
		2	6.0	264 ± 22	204 ± 17	11 ± 5	340 ± 24	53 ± 13	62 ± 23
		3	3.5	235 ± 20	201 ± 17	19 ± 6	208 ± 16	44 ± 13	46 ± 16
		4	3.5	359 ± 41	240 ± 29	19 ± 9	431 ± 46	82 ± 23	114 ± 53
		5	2.3	239 ± 21	205 ± 18	14 ± 6	337 ± 25	59 ± 14	35 ± 26
		6	1.0	325 ± 20	178 ± 13	14 ± 4	345 ± 20	38 ± 10	43 ± 19
		7	2.0	238 ± 19	200 ± 16	7 ± 5	356 ± 23	51 ± 12	84 ± 26
		8	3.0	277 ± 17	217 ± 15	16 ± 5	417 ± 24	46 ± 10	82 ± 22
		9	3.0	299 ± 18	217 ± 14	14 ± 4	403 ± 22	53 ± 10	75 ± 20
C	4/9/76	1	4.0	394 ± 34	144 ± 12	25 ± 8	533 ± 40	45 ± 14	47 ± 32
		2	6.0	324 ± 14	177 ± 8	18 ± 3	453 ± 16	37 ± 6	29 ± 14
		3	6.0	291 ± 18	191 ± 13	16 ± 5	385 ± 20	36 ± 9	18 ± 20
		4	6.0	344 ± 25	223 ± 18	27 ± 7	473 ± 12	46 ± 11	56 ± 27
		5	6.0	352 ± 43	246 ± 32	27 ± 12	482 ± 51	55 ± 20	45 ± 52
		6	5.0	287 ± 25	201 ± 19	33 ± 8	413 ± 13	40 ± 13	67 ± 31
		7	6.0	302 ± 38	186 ± 26	33 ± 12	454 ± 47	21 ± 17	48 ± 47
		8	6.0	372 ± 30	272 ± 30	19 ± 7	394 ± 29	29 ± 12	36 ± 32
		9	6.0	251 ± 21	201 ± 17	28 ± 7	321 ± 22	30 ± 11	31 ± 25
		10	4.5	254 ± 27	255 ± 26	23 ± 9	337 ± 30	9 ± 15	0 ± 32
		11	4.0	328 ± 32	173 ± 20	11 ± 7	456 ± 40	71 ± 18	82 ± 35
D	5/21/76	1	6.0	307 ± 23	195 ± 17	71 ± 10	454 ± 29	38 ± 12	13 ± 25
		2	9.0	276 ± 25	201 ± 19	51 ± 9	414 ± 30	19 ± 12	0 ± 27
		3	4.0	295 ± 36	266 ± 32	80 ± 16	451 ± 44	32 ± 17	0 ± 38
		4	4.0	295 ± 46	229 ± 37	116 ± 24	480 ± 61	29 ± 22	21 ± 52
		5	5.0	319 ± 28	143 ± 17	109 ± 14	460 ± 34	28 ± 13	13 ± 33
		6	6.0	306 ± 41	236 ± 33	75 ± 18	428 ± 49	29 ± 20	33 ± 53
E	5/11/76	1	5.0	357 ± 34	162 ± 20	69 ± 12	557 ± 44	19 ± 14	13 ± 33
		2	2.0	446 ± 31	219 ± 18	72 ± 9	637 ± 38	27 ± 11	3 ± 22
		3	2.0	465 ± 33	210 ± 19	84 ± 11	592 ± 38	48 ± 13	11 ± 24
		4	2.0	430 ± 32	214 ± 19	77 ± 10	606 ± 39	27 ± 12	34 ± 25

Normal cytoplasmic elemental concentrations of 34 fibers from four frog toe muscles and one frog semitendinosus muscle (D). Muscles from frogs A, B, and D had 4% bovine serum albumin added to the Ringer's solution. All muscles were exposed to 10^{-6} M TTX. Each concentration represents one analysis with its standard deviation. For a discussion of the SD, see Materials and Methods (statistics section).

absolute amounts of Na and Cl contained in the vacuoles were significantly greater than in the same volume of cytoplasm. The analyses of the contents adhering to the edge of broken vacuoles probably included a small volume of adjacent cytoplasm.

The vacuoles in muscles treated with hypertonic NaCl, with one exception, did not contain detectable concentrations of sequestered calcium. The minimal detectable concentration of Ca with the probe parameters used was 15 mmol/kg. Ca granules were frequently found in the longitudinal SR of these muscles treated with hypertonic solutions (see below).

TABLE II

Summary of Elemental Analysis of Normal Muscles

Element	Frog	No. of fibers	Weighted $\bar{x}$ ± SEM	*P* value for χ_ν^2‡	Grand weighted $\bar{x}$ ± SEM ± SD*	*P* value for χ_ν^2§	Analysis of variance *P* value of F ratio
P	A	4	311 ± 18.9	0.8			
	B	9	273 ± 6.7	0.01			
	C	11	310 ± 7.2	0.001	302 ± 4.3 ± 51.3	<0.001	<0.001
	D	6	299 ± 12.3	0.9			
	E	4	426 ± 16.0	0.1			
S	A	4	125 ± 9.6	0.6			
	B	9	204 ± 5.3	0.5			
	C	11	187 ± 4.7	0.01	189 ± 2.9 ± 33.4	<0.001	<0.05
	D	6	192 ± 9.0	0.01			
	E	4	202 ± 9.5	0.1			
Cl	A	4	56 ± 6.0	0.05			
	B	9	14 ± 1.6	0.8			
	C	11	21 ± 1.9	0.5	24 ± 1.1 ± 20.1	<0.001	<0.001
	D	6	73 ± 5.3	0.01			
	E	4	75 ± 5.2	0.8			
K	A	4	383 ± 20.8	0.9			
	B	9	336 ± 7.5	<0.001			
	C	11	427 ± 6.2	<0.001	404 ± 4.3 ± 84.5	<0.001	<0.001
	D	6	444 ± 15.1	0.9			
	E	4	600 ± 20	0.6			
Mg	A	4	49 ± 10.0	0.8			
	B	9	48 ± 3.9	0.8			
	C	11	37 ± 3.4	0.4	39 ± 2.1 ± 12.3	>0.5	<0.01
	D	6	29 ± 6.0	0.9			
	E	4	30 ± 6.2	0.4			

Summary of elemental analyses of the normal muscles shown in Table I.

* Formulae for weighted mean, SEM. and SD are given in Materials and Methods (statistics section).

‡ χ_ν^2 reduced chi square *P* values of the distribution of the concentrations measured within one muscle.

§ χ_ν^2 reduced chi square *P* values of the distribution of the concentrations measured in all the muscles.

Electron Probe Analysis of Muscles Incubated in Hypertonic 350 mM Sucrose Solution

Large-spot analysis of muscles treated with hypertonic sucrose solution gave the following weighted mean concentration for nine fibers from winter frogs (mmol/kg dry wt ± SEM): Na, 131 ± 12; P, 392 ± 11; S, 236 ± 7; Cl, 23 ± 2; K, 440 ± 12; Mg, 71 ± 6; and for 10 fibers from summer frogs: Na, 48 ± 9; P, 467 ± 10; S, 239 ± 5; Cl, 18 ± 2; K, 580 ± 10; Mg, 50 ± 4. In six fibers in one of the above muscles not included in the mean values given above, the K concentrations were low (167–317 mmol/kg dry wt) and the Na concentrations were high (148–228 mmol/kg dry wt). The Cl concentrations (13–34 mmol/kg dry wt) were within normal limits. It is possible that the high Na in these fibers was related to the occasional depolarizing effect of hypertonic solutions observed by others (9).

The K/Cl ratios in paired analysis of 24 vacuoles and adjacent cytoplasm were, respectively, 4.8 ± 1.1 SE and 28.4 ± 5.3 SEM, $P < 0.001$. The NaCl ratio in the same paired analyses was 2.0 over the vacuoles and 5.6 over the cytoplasm. Using the same probe current and microvolume analyzed, the absolute number of Cl counts over the vacuoles was significantly greater ($P < 0.01$) than over the cytoplasm. These findings show that the Cl concentration was higher in the vacuoles than in the cytoplasm, and that this difference in

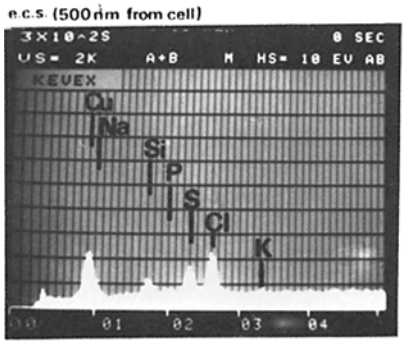

ML FOR FILE 29 TIME=300
CONT AREA = 1763 ± 63

ELEMENT	CONC (mM/KG)	PEAK CNT	PEAK ERROR
Na	290.9 ± 45.7	918 ± 140	
Mg	−16.5 ± 14.3	−120 ± 103	
P	45.3 ± 11.5	561 ± 142	
Cl	344.8 ± 16.8	5566 ± 183	
K	17.4 ± 8.4	290 ± 141	
Ca	6.6 ± 8.1	116 ± 142	

CHISQD = 2.97

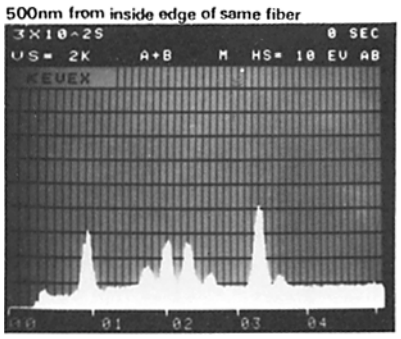

ML FOR FILE 30 TIME = 300
CONT AREA = 2631 ± 76

ELEMENT	CONC (mM/KG)	PEAK CNT	PEAK ERROR
Na	33.8 ± 33.2	159 ± 156	
Mg	33.2 ± 11.2	360 ± 121	
P	350.1 ± 14.6	6475 ± 193	
Cl	75.6 ± 7.8	1821 ± 180	
K	496.6 ± 17.0	12359 ± 224	
Ca	2.9 ± 6.6	77 ± 173	

CHISQD = 3.74

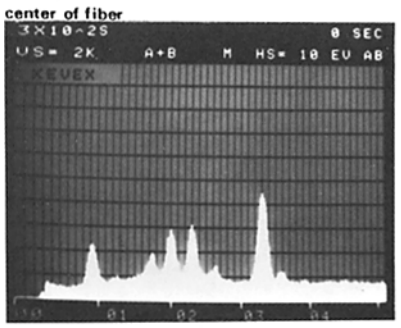

ML FOR FILE 33 TIME= 300
CONT AREA = 3134 ± 79

ELEMENT	CONC (mM/KG)	PEAK CNT	PEAK ERROR
Na	27.9 ± 26.7	156 ± 150	
Mg	31.9 ± 9.7	411 ± 125	
P	308.1 ± 12.0	6785 ± 201	
Cl	58.3 ± 6.5	1672 ± 182	
K	475.9 ± 14.3	14102 ± 227	
Ca	−9.9 ± 5.4	−307 ± 169	

CHISQD =3.78

17

FIGURE 17 X-ray spectra and elemental concentrations from two areas of the same fiber and the adjacent extracellular space.

concentrations was not due merely to variations in the relative dry mass of the two regions.

An example of analysis of a muscle incubated in hypertonic sucrose solution is shown in Table V and Fig. 15 and also illustrates the sharp ionic gradients across membranes at 100 nm spatial resolution. The Cl, as well as the absolute number of Cl counts, was significantly higher and the K and K counts were lower in the lumen of the six vacuoles analyzed than over the adjacent cytoplasm. Analysis of the lumen of the oval structure labeled 1 showed (mmol/kg dry wt ± SD) 122 ±

TABLE III

Elemental Concentrations of Terminal Cisternae and Cytoplasm in Normal Frog Toe Muscles

No. of analyses summed	Cytoplasm							Terminal cisternae						
	Na	Mg	P	S	Cl	K	Ca	Na	Mg	P	S	Cl	K	Ca
	mmol/kg dry wt ± SD													
5	62 ± 49	57 ± 22	544 ± 63	241 ± 34	66 ± 16	782 ± 80	15 ± 11	50 ± 38	30 ± 16	682 ± 61	202 ± 25	71 ± 14	778 ± 65	61 ± 12
5	103 ± 34	58 ± 14	352 ± 30	263 ± 23	45 ± 9	519 ± 36	−4 ± 6	41 ± 30	24 ± 12	424 ± 32	246 ± 21	42 ± 9	597 ± 39	77 ± 10
4	137 ± 60	31 ± 20	469 ± 56	191 ± 30	26 ± 13	577 ± 62	1 ± 10	122 ± 69	34 ± 24	550 ± 74	204 ± 36	43 ± 17	607 ± 76	40 ± 16
4	−6 ± 26	33 ± 11	242 ± 20	208 ± 17	28 ± 7	394 ± 25	−1 ± 5	26 ± 33	48 ± 14	460 ± 36	198 ± 20	52 ± 10	534 ± 38	81 ± 12
6	−36 ± 24	34 ± 11	310 ± 23	197 ± 16	59 ± 9	519 ± 31	1 ± 5	41 ± 25	52 ± 11	414 ± 26	193 ± 15	63 ± 8	580 ± 32	60 ± 8
6	69 ± 26	36 ± 10	420 ± 43	227 ± 25	44 ± 8	568 ± 54	2 ± 4	57 ± 46	52 ± 21	377 ± 71	279 ± 54	51 ± 16	497 ± 87	65 ± 18
Weighted $\bar{x}$	29	39	317	216	42	488	1	44	40	449	208	54	587	66
SEM	12 6	5.2	12.3	8.8	3.8	15.5	2.3	14.1	5.9	16.0	9.1	4.5	18.7	4.6

Elemental concentrations of terminal cisternae and cytoplasm in normal frog toe muscles, determined by paired small-spot electron probe analysis (~50 nm) using identical probe parameters. The number of spectra obtained during 100-s counts is shown in the first column. The quantitation program was run on the summed spectra. Muscles were incubated in Ringer's with 10^{-6} M TTX for 2 h 40 min without bovine serum albumin. For weighted $\bar{x}$, SEM, and negative values, see Materials and Methods.

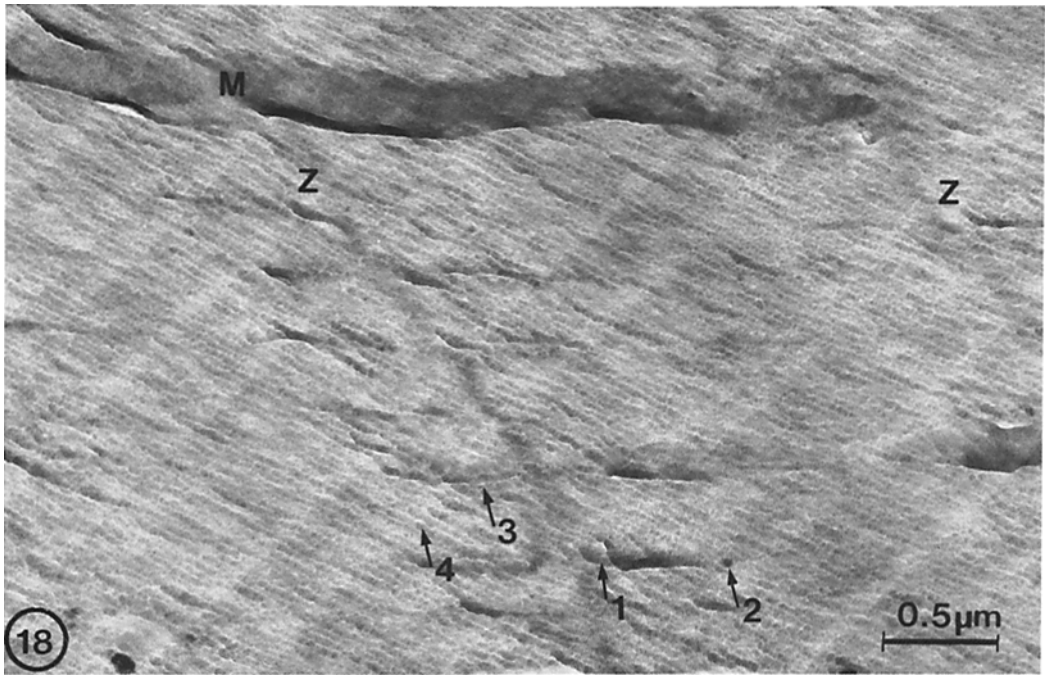

FIGURE 18 Frozen-dried section of normal frog toe muscle. Analyses were done using 50 nm probe sizes at the regions indicated by arrows. The large standard deviations shown below reflect the short counting times (100 s). Four to six analyses of this type were summed for use in Table III. Unstained. × 30,000. Elemental concentrations (mmol/kg dry wt ± SD) of the areas numbered *1* through *4*:

no.	P	K	Cl	Ca	Mg
1	582 ± 148	589 ± 161	49 ± 39	0 ± 26	21 ± 51
2	949 ± 289	587 ± 186	37 ± 41	375 ± 130	71 ± 75
3	562 ± 168	497 ± 143	24 ± 33	101 ± 52	38 ± 56
4	376 ± 103	498 ± 117	30 ± 29	0 ± 20	32 ± 44.

30 Cl and 59 ± 18 K, while the cytoplasm at about 200 nm distance away contained 6 ± 13 Cl and 428 ± 62 K. Comparison of areas 1 and 4 separated by ~100 nm also shows sharp gradients. In analyses 4 and 15 over the vacuole membrane, more phosphorus was detected than over the cytoplasm. The phosphorus in the lumen of these structures was significantly lower than over the cytoplasm.

Electron Probe Analysis of Muscles Incubated in Hypertonic Na Isethionate

The purpose of this experiment was to determine, by measuring the S X-rays, whether the impermeant anion isethionate entered the vacuoles. The results of analysis of 4.8-μm diameter regions of nine fibers incubated for 30 min in 2.2 × hypertonic Na isethionate solution were (values expressed as mmol/kg dry wt ± SEM): Na, 119 ± 12; P, 416 ± 12; S, 231 ± 8; Cl, 17 ± 3; K, 521 ± 13; and Mg, 43 ± 5. The normal cytoplasmic S values confirm that the plasma membrane effectively excludes isethionate. In two sets of analyses over 2- and 4-μm diameter areas, the areas which included prominent vacuoles as well as cytoplasm had 18 and 44 mmol/kg dry wt more Na and 20 mmol(kg dry wt more S than the neighboring areas that did not contain obvious vacuoles. Analysis with a focused probe of 80 nm over one of these same vacuoles showed (mmol/kg dry wt) S, 403 ± 37 SD; and Na, 478 ± 69 SD, indicating the entry of Na isethionate. The K/S ratios in 12 paired analyses over vacuoles and adjacent cytoplasm were, respectively, 1.7 ± 0.65 SD and 2.6 ± 0.8 SD. The K/Na ratios in the same paired analyses were 3.0 ± 1.4 SD over vacuoles and 7.1 ± 4.8 SD over cytoplasm ($P < 0.001$).

The external solution contained 272 mM Na and 5.4 mM Cl ($CaCl_2$ and KCl) or a Na/Cl ratio

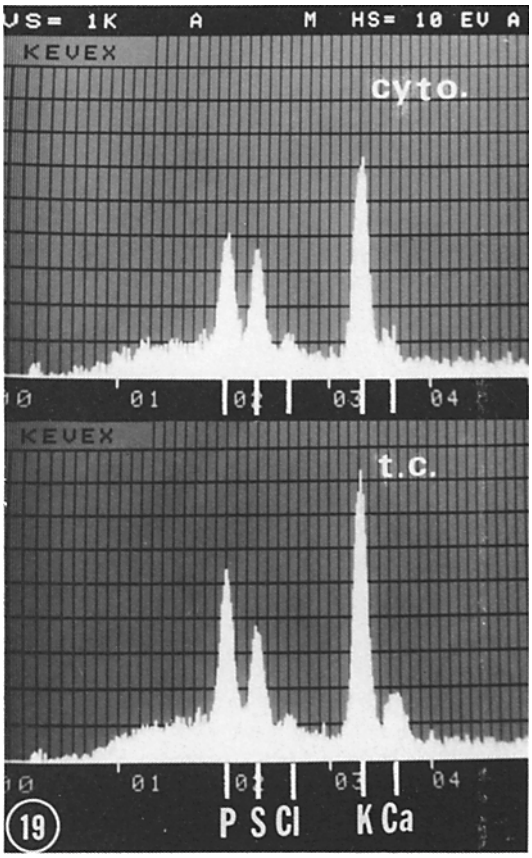

FIGURE 19 X-ray spectra over terminal cisternae and adjacent cytoplasm of normal frog toe muscle. Each spectrum represents the sum of five analyses of 100 s each. The ordinate gives the number of counts for the energies shown on the abscissa in keV. Note the presence of a Ca peak in the spectrum recorded from terminal cisternae. The K K_β at 3.59 keV is separated from the Ca K_α by 100 eV. Instrument and the extraneous continuum were subtrated by the computer program.

of 50. Even if all of the Na (119 mM/kg dry wt) analyzed in the fiber had been in an extracellular compartment, the Cl associated with it should have been only ~2mmol/kg dry wt. The Cl values were greater than this in six of the nine fibers analyzed, suggesting that Cl was retained in some of the fibers.

Granules consisting of Ca, P, and Mg were found in the longitudinal SR of all fibers analyzed. The ratios of these elements in the granules are summarized in the next section.

Ca Granules

Electron-opaque granules (Fig. 16) were found in every fiber examined that had been exposed to hypertonic NaCl, hypertonic sucrose, or hypertonic Na isethionate solution. They were associated with the SR and were most frequently in the longitudinal elements. An occasional granule was also found in the control fibers. The results of all granule analyses were used to determine their composition. The granules consisted of Ca, Mg, and P. The mean ratio of Ca/Mg in 28 analyses was 6.1 ± 2.4 SD. To estimate the ratio of Ca plus Mg to P, the P concentration was corrected for P counts originating from cytoplasmic P (but not for P in SR membrane phospholipids) included in the area analyzed by scaling the P to the K on the basis of the P/K over the cytoplasm. The corrected mean (Ca + Mg)/P was 1.1 ± 0.35 SD. A spectrum from one of these granules in a muscle fiber incubated in hypertonic NaCl solution is shown in Fig. 21.

DISCUSSION

Cryoultramicrotomy and Electron Probe Analysis

The most general conclusions reached through this study are: that it is feasible to freeze intact cells without cryoprotection while preserving ultrastructure and the boundaries of ion distribution, and that the results of electron probe quantitation of cryo sections are consistent with the known intracellular concentrations of the detectable elements (see below).

It should be emphasized that great care needs to be taken during dissection to avoid damage even to the most superficial portions of the tissue to be frozen for cryoultramicrotomy, since only the most superficial regions yield cryo sections sufficiently free of ice crystals to be suitable for high resolution imaging and electron probe analysis. A spatial X-ray resolution of at least 100 nm for the distribution of diffusible elements (K, Cl) can be demonstrated across membrane-bounded compartments in frozen-dried ultrathin cryo sections (Table V and Fig. 15). Other techniques, involving the use of fixatives, negative stains, and freeze substitution, may yield sections showing more ultrastructural detail than frozen-dried cryo sections prepared in the manner described in this study. However, they caused translocation and loss of diffusible elements (86, 90), and are not suitable for quantitative electron probe analysis of diffusible ions. A disadvantage of the freeze-drying process is that the quantitative comparison of solute

TABLE IV

Elemental Concentrations of Fibers Exposed to 2.2 × Hypertonic NaCl Solution

Frog	Fiber no.	No. of analyses	Na	P	S	Cl	K	Mg
					mmol/kg dry wt			
3/5/76	1	6	180 ± 28	316 ± 30	298 ± 24	23 ± 5	441 ± 32	103 ± 16
	2	4	236 ± 24	562 ± 28	134 ± 10	30 ± 5	583 ± 27	71 ± 9
	3	1	208	325	293	9	498	125
12/11/75	1	3	51 ± 18	442 ± 25	259 ± 16	21 ± 5	633 ± 32	56 ± 11
	2	2	108 ± 32	344 ± 29	185 ± 18	17 ± 7	391 ± 29	57 ± 16
3/3/76	1	4	69 ± 28	334 ± 26	181 ± 16	31 ± 6	458 ± 31	38 ± 13
	2	6	117 ± 24	319 ± 20	223 ± 15	41 ± 6	419 ± 23	54 ± 12
	3	5	70 ± 13	310 ± 11	217 ± 8	22 ± 3	471 ± 15	52 ± 6
	4	2	62 ± 36	315 ± 32	270 ± 27	39 ± 9	513 ± 44	65 ± 19
1/9/76	1	9	127 ± 12	289 ± 10	232 ± 8	39 ± 3	382 ± 11	48 ± 6
	2	6	95 ± 16	313 ± 15	242 ± 12	24 ± 4	487 ± 20	63 ± 9
5/25/76	1	3	46 ± 21	349 ± 19	203 ± 13	31 ± 5	487 ± 23	29 ± 8
	2	6	40 ± 15	389 ± 16	233 ± 11	27 ± 4	563 ± 20	33 ± 6
	3	1	10	298	204	29	372	25
	4	1	78	401	257	25	500	38
	5	1	58	295	240	6	507	43

Summary of 60 large spot (0.5-14 μm diam) electron probe analyses of frog toe muscles incubated in 2.2 × hypertonic NaCl solution. Each row represents one fiber. Weighted means and standard errors of the weighted means are shown for fibers in which more than one analysis was done.

concentrations between compartments having different (and unknown) degrees of hydration becomes difficult and that the contents of highly aqueous domains (vacuoles, the lumen of secretory structures, and capillaries) are precipitated on the limiting wall during drying. Therefore, for the quantitative analysis of highly aqueous domains the use of frozen-hydrated (44, 65), rather than frozen-dried, cryo sections may offer some advantages, in spite of the increased technical difficulties and the reduced sensitivity of electron probe analysis due to the background (continuum counts) generated by ice.

The analytical sensitivity of energy-dispersive detectors suitably mounted on a transmission electron microscope with optimized design is sufficient to detect during a 100-s count, a minimal detectable concentration of 10 mM K/kg dry wt in a 50-nm diameter region of a 100-nm thick section (83, 84). The minimal detectable mass (in the absence of significant background due to organic matrix) is $\sim 10^{-19}$–10^{-20} g of iron (82, 83). As shown elsewhere in detail (Fig. 6 in reference 83), these detection efficiencies vary but little for biological elements in the periodic table down to and including P. However, the sensitivity and, therefore, also the precision, for measuring elements having a lower atomic number (e.g., Mg and Na) are significantly worse due to the very marked absorption of the softer X-rays, emitted by these elements, in the beryllium window of the detector. The minimal detectable concentration can obviously be reduced by increasing beam current, prolonging analysis time, or using thicker sections. However, the first two approaches increase the potential for radiation damage while the use of thick sections will reduce spatial X-ray and image resolution. For the measurement of bulk cellular Na at a relatively low (micron) spatial resolution, the use of thicker sections (72) may be preferable. However, X-ray absorption within the specimen, negligible in ultrathin sections, is significant and has to be corrected for if section thickness exceeds the mass equivalent of a 0.5 μm-thick plastic specimen (83).

Quantitative electron probe analysis based on the method used in this study (45, 83, 84) requires the accurate determination of the characteristic counts and also the X-ray continuum counts used as a measure of the dry mass of the biological

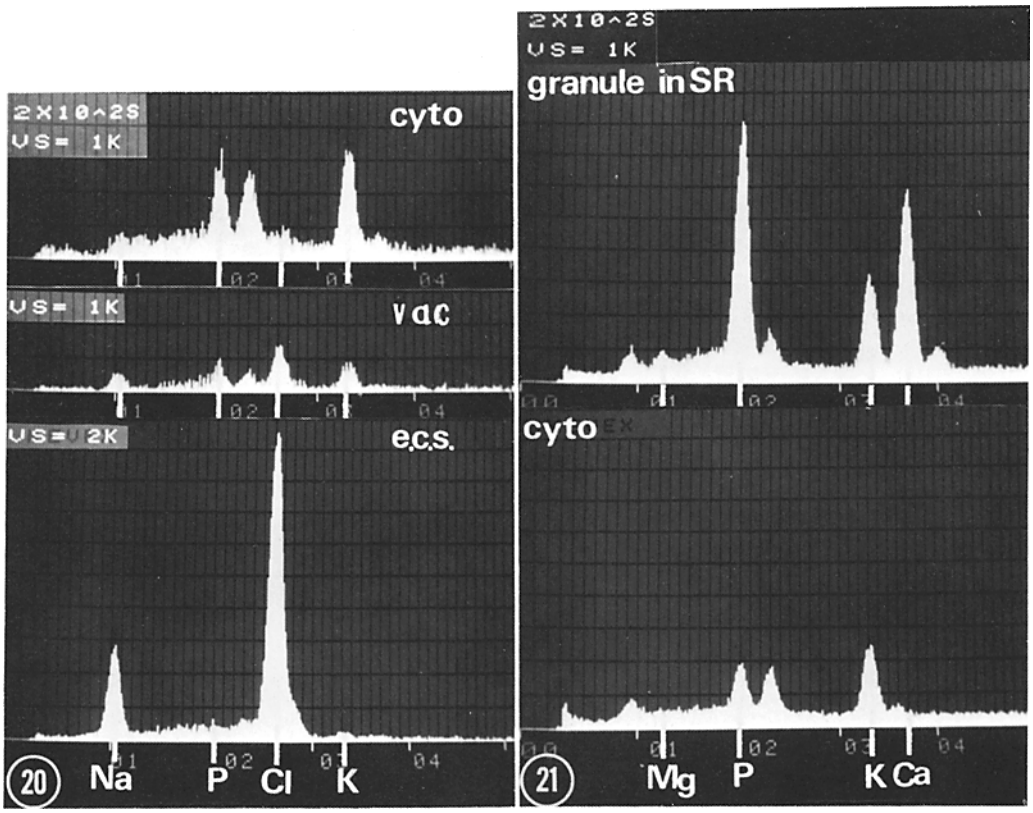

FIGURE 20 X-ray spectra of the cytoplasm (*cyto*) vacuole (*vac*), and extracellular space (*e.c.s.*) from a frozen-dried thin section of a frog toe muscle incubated in 2.2 × hypertonic NaCl. The ordinate gives the number of counts for the energies shown on the abscissa. The positions of the characteristic energies of Na, P, Cl, and K are indicated. Note the NaCl peaks over the vac and the e.c.s. Instrument and osmium peaks, and the extraneous continuum were subtracted by the computer program.

FIGURE 21 X-ray spectra of the cytoplasm (*cyto*) and a granule in the longitudinal SR from a muscle exposed to 2.5 × hypertonic sucrose. Note the Ca, P, and Mg peaks from the granule.

matrix. In the presence of overlapping peaks (e.g., the Na K and Cu L and the K K_β and Ca K_α peaks) it is necessary to use computer-based spectrum fitting techniques to deconvolute and obtain the respective counts in the adjacent characteristic peaks. Similarly, since extraneous sources (e.g., grid, specimen holder, parts of electron microscope column) can also contribute to the X-ray continuum, these extraneous contributions have to be subtracted to obtain the continuum X-rays arising from the specimen itself. In the method used in the present study, the extraneous continuum generated by the grid can be scaled accurately to the Cu peak emitted from the same source, and is subtracted by the computer fitting routine. Thus, since the multiple least squares fitting technique easily permits the separation of the adjacent Cu L and Na K lines, we used copper grids to obtain an accurate correction for the grid-generated continuum (83). This approach has the disadvantage of a relatively high count rate due to the copper grid. Without a reliable method of deconvoluting the adjacent Cu L and Na K peaks, the presence of the Cu signal would preclude the quantitation (or even the detection) of Na (c.f. Fig. 17).

The ultimate limit on the sensitivity and spatial resolution of biological electron probe analysis is that imposed by radiation damage (for review, see reference 84). Fortunately, when sufficient mass loss (10–20%) occurs to cause an error greater than that inherently due to count statistics, there is visible lightening of the specimen (83). Similarly, a significant gain in mass due to contamination

TABLE V

Ion Compartmentalization in a Fiber Exposed to 2.5 × Hypertonic Sucrose

No.	Region analyzed	Counting time	P		Cl		K		Mg	
		s	*mmol/kg dry wt ± SD*	*counts*	*mmol/kg dry wt ± SD*	*counts*	*mmol/kg dry wt ± SD*	*counts*	*mmol/kg dry wt ± SD*	*counts*
1	Lumen	100	44 ± 23	191	122 ± 30	672	59 ± 18	335	45 ± 31	91
2	Cytoplasm	100	309 ± 54	1,735	6 ± 13	36	428 ± 62	3,004	78 ± 33	194
3	Membrane	100	232 ± 38	1,492	71 ± 18	585	202 ± 31	1,715	21 ± 24	64
4	Membrane	100	652 ± 85	4,228	17 ± 13	142	391 ± 18	3,328	51 ± 28	155
5	e.c.s.	100	41 ± 30	127	1,301 ± 240	5057	60 ± 35	239	−3 ± 36	−5
6	Lumen	200	22 ± 11	239	117 ± 17	1,632	12 ± 7	168	23 ± 18	122
7	Cytoplasm	200	252 ± 30	2,881	10 ± 8	145	324 ± 32	4,874	66 ± 21	353
8	Lumen	200	2 ± 10	20	121 ± 18	1,557	1 ± 7	15	16 ± 18	79
9	Cytoplasm	200	442 ± 48	4,649	24 ± 9	316	336 ± 37	4,647	74 ± 24	363
10	Lumen	200	−10 ± 9	−155	117 ± 17	1,646	7 ± 7	105	14 ± 17	74
11	Cytoplasm	200	363 ± 38	4,503	19 ± 9	300	431 ± 40	6,999	79 ± 22	462
12	Lumen	200	29 ± 11	382	115 ± 15	1,972	27 ± 7	472	−2 ± 11	−18
13	Cytoplasm	200	263 ± 28	3,109	24 ± 9	372	321 ± 29	5,100	37 ± 15	259
14	Membrane	200	214 ± 27	2,127	42 ± 11	538	283 ± 28	3,787	45 ± 16	260
15	Membrane	200	494 ± 39	7,716	44 ± 9	895	395 ± 31	8,300	52 ± 14	477
16	Lumen	100	253 ± 42	1,420	77 ± 20	551	212 ± 33	1,564	20 ± 24	50
17	Cytoplasm	100	330 ± 55	1,742	14 ± 13	91	430 ± 62	2,981	80 ± 33	199

Ion compartmentalization in a fiber incubated in 2.5 × hypertonic sucrose solution. Analyses were done at −110°C using probe diameters of ~70-100 nm, on an unstained, frozen-dried section without a carbon foil support. Counts = number of characteristic counts in a given peak without the underlying background. Lumen and membrane refer to respective components of the swollen structures; e.c.s., extracellular space. Ca was below the levels detectable (15 mmol/kg) with the probe parameters used. Counting statistics for Na were not adequate due to the short counting times and small probe currents (see Fig. 15).

also leads to a visible contamination spot in the image. Thus, by avoiding the use of visibly etched or contaminated areas for quantitative electron probe analysis, the errors in concentration measurements can be reduced to 15% or less (83).

Normal Muscle

THE TRIAD AND THE COMPOSITION OF THE TERMINAL CISTERNAE: The morphology of the triadic junction in cryo sections was similar to the configuration observed in glutaraldehyde-osmium-fixed and plastic-embedded material (38-40, 74). The flattened shape of the T tubule, the 12-nm junctional gap, and the suggestion of foot processes at the triadic junction seen in our frozen-dried material indicate that the morphology of these structures is not due to fixation and dehydration. The existence of the junctional gap in unfixed material is of particular interest, as this is the site that must be traversed by the signal for Ca release.

An important result of this study is the finding that the Cl content of the normal terminal cisternae does not resemble that of the extracellular space, but is similar to the cytoplasmic concentration. The slightly higher Na and Cl concentrations detected over the terminal cisternae than over the cytoplasm were within statistical error, and even this trend could be due to Cl X-rays generated from adjacent T tubules. If the SR contained Na Cl similar to the extracellular concentrations as proposed previously (46, 79), then the Cl content of the terminal cisternae would be ~360 mmol/kg dry wt. The 54 mmol Cl/kg dry wt measured in this study (Table II) are very significantly less than this calculated value. Therefore, these findings suggest that in the normal resting muscle the ionic composition of the SR is not similar to that of the extracellular space. The slow component of Cl efflux (46) could be originating from the SR having a Cl concentration similar to that of the cytoplasm. However, the absence of "extracellular" Cl within the terminal cisternae of normal muscle does not completely exclude the possibility that the normal T tubule-SR junction is permeable to Cl, but that the mobile anion is partially excluded from the SR lumen by the Donnan effect of negatively charged proteins (68). The somewhat (~20%) higher K concentration in the terminal cisternae than in the cytoplasm may be due to the binding of this cation to calsequestrin (21, 68).

Sequestered Ca was found in the terminal cister-

nae in normal resting muscle. However, not every area identified by its image as a terminal cisterna contained detectable Ca. This lack of Ca could be due to incorrect structural identification, such as mistaking glycogen-containing spaces for terminal cisternae in the unstained sections, or to analyses of regions that contained only a small fraction of a terminal cisterna within the section. It is also possible that not all terminal cisternae contain detectable Ca at a given time. The mean Ca of 66 ± 4.6 SEM mmol/kg dry wt (≃16 mmol/1 SR) measured in the terminal cisternae in the present study is well within the range of 5–40 mmol/1 SR estimated with other techniques (32, 37, 75, 98, 99), and dependent on the assumptions made about how calcium is distributed (e.g., whether in 13 or 5% of fiber volume). However, due to the combined effects of count statistics and beam damage (83), the results of electron probe analysis with the small probes required for analyzing individual terminal cisternae may be subject to greater error (~20%) than the results of large-probe analyses. Although some of these errors were minimized by terminating analysis before visible etching occurred, it would be preferable to perform further analyses at better vacuum and lower temperatures to obtain the absolute value of the calcium content of terminal cisternae.

FIBER COMPOSITION: The Cl content of the muscle fibers measured with electron probe analysis was 24 mmol/kg dry wt ± 1.1 SEM and also showed some variations between frogs (see Tables I and II) that may have been seasonal or due to differences in the incubation times in Ringer's solution (13, 46). Since the Cl concentration measured with large-diameter (0.5–9 μm) probes may have included Cl sequestered in organelles, we have also determined the Cl concentration with small-diameter probes (50–100 nm) in cytoplasm excluding organelles (terminal cisternae, mitochondria, nuclei) and in the organelles themselves. The cytoplasmic Cl concentrations measured with small- or large-diameter probes in the same fiber were not significantly different. The organelles analyzed showed no compartmentalization of Cl. In fact, the mitochondria appeared to partially exclude Cl in striated, as in smooth (88), muscle. A relatively low permeability of the mitochondrial membrane to Cl has previously been demonstrated in isolated liver mitochondria (97). Thus, our results indicate a relatively high (see below) total cytoplasmic Cl.

The results of earlier bulk chemical measurements, showing a cellular Cl content (e.g., 41 mmol/kg dry cell [46]) significantly in excess of the 9 mmol/kg dry wt calculated on the basis of passive distribution (2), led to the suggestion that the "excess Cl" in frog striated muscle was compartmentalized in the SR (46, 79). However, recent studies with Cl-sensitive electrodes (7, 58) indicate that the cytoplasmic Cl is greater than can be accounted for by a passive (18, 48) distribution. For example, in frog muscles bathed in Ringer's solution the resting membrane potential was 82.7 mV ± 7.0 SD and the Cl activity, 7.0 mmol/liter cell H_2O ± 2.4 SD, as compared to a calculated value of passively distributed $[Cl]_i$ of 3.3 mmol/kg cell water (7). The 28 mmol Cl/kg dry wt ± 11.7 SD (assuming 75% cell H_2O and a Cl activity coefficient of 0.75) obtained in the latter study are in very good numerical agreement with the 24 ± 20.1 mmol/kg dry wt measured with electron probe analysis (present study). However, in view of the significant frog-to-frog variations in Cl content, the very good agreement between the two sets of results may be fortuitous.

The excess Cl present in frog striated muscle fibers incubated in normal Ringer's solution (K_o = 3 mmol/liter) is suggestive of a nonDonnan distribution of this anion in muscles bathed in low K media. An even greater departure of $[Cl]_i$ from the passive distribution has been observed in other cell systems. The 60 mmol/kg fiber water (180 mmol/kg dry wt) $[Cl]_i$ in vertebrate smooth muscle (22, 55, 57) suggests a discrepancy of 20–40 mV between E_{Cl} and E_m; a passive, Boyle-Conway type distribution of Cl is not observed in smooth muscle until K_o is raised to 50 mM or higher (55). There is a similarly large discrepancy between E_m and E_{Cl} in squid (59, 96) and in crayfish (93) giant axons. Very recently, an ATP-dependent Cl transport into dialyzed squid axons has been demonstrated (80). It is possible that an active inward Cl transport system is also operating in frog striated muscle, but its contribution to Cl distribution is detectable only at relatively low (<5 mM) extracellular K concentrations.

The K content of the control muscle fibers (404 mmol/kg dry wt ± 4.3) determined by electron probe analysis was consistent with previous chemical determinations of 365–420 mmol K/kg dry wt (1, 14, 18, 47, 66). The frog-to-frog variations in K are in agreement with the highly significant differences in the resting membrane potentials between frogs (1) and with the 137 ± 26 SD mmol K/kg fiber H_2O (≃411 ± 80.4 SD mmol/kg dry

wt) measured in single frog semitendinosus fibers with neutron activation analysis (47). However, because the concentrations measured with electron probe analysis of frozen-dried cryo sections are on a dry weight basis, the fibers in which the concentrations of all elements in the water phase deviate in the same direction from the mean could differ in their cell water content and have the same ionic distributions (activities in cell H_2O) and resting membrane potentials. In fact, it is apparent from Table II that the frogs with the higher K contents also have higher Cl contents.

The phosphorus content (320 mmol/kg dry wt) quantitated in normal muscles with electron probe analysis is in substantial agreement with the results of chemical analysis of total P (up to 300 mmol/kg dry wt) in muscle extracts (92). The phosphate metabolites as determined by ^{31}P-nuclear magnetic resonance (NMR) account for only about 135 mmol/kg dry wt muscle P (20) and actomyosin-bound P for another ~7 mmol/kg (8); a significant proportion of the remaining cytoplasmic P in muscle can be accounted for by the ~60 mmol P/kg dry wt in phospholipids (M. Bárány, personal communication).

The mean Mg content of the fibers was 39 ± 2.1 SEM mmol/kg dry wt, and there was little fiber-to-fiber variation within one muscle as indicated by the probability values for χ_ν^2 in Table II. The values are similar to those reported for whole frog (13, 43) sartorius muscle (8.6 ± 0.3 SEM mmol/kg wet wt ≃40 mmol/kg dry cell in reference 13), and for the cellular Mg content of unperfused rat ventricle (41.4 ± 0.3 mmol/kg dry wt in reference 73). Ionized Mg in skeletal muscle is probably less than 1 mM (35).

The Na_i determined by electron probe analysis (42 ± 4.4 SEM mmol/kg dry wt) showed considerable fiber-to-fiber and muscle-to-muscle variation (c.f. Table I and II), and was within the range of the 31–87 mmol/kg dry wt values obtained with bulk chemical analyses (6, 61, 85) and the 78 mmol/kg dry wt ± 30.9 SD measured with neutron activation analysis of single fibers (47). Due primarily to the absorption of the relatively soft Na X-rays in the beryllium window of the detector, the statistical error of the electron probe measurements is relatively large (83), and longer counting times (or higher probe currents) will be required for improving the precision of Na measurements. However, the results of bulk chemical analysis, neutron activation, and electron probe analysis are all compatible with a higher cytoplasmic Na concentration than the 16–27 mmol/kg dry wt detectable with Na-sensitive electrodes (6, 61, 67). In view of the significant fiber-to-fiber and frog-to-frog variations in total fiber Na content, an accurate estimate of bound Na (the difference between total $[Na]_i$ and the cytoplasmic free Na) would require that studies with Na-selective electrodes and with electron probe analysis be performed on the same muscle fibers. Electron probe analysis of nuclei, mitochondria, and terminal cisternae showed no evidence of compartmentalization of Na. No definite statement can be made about the absolute Na concentrations in these organelles, due to the large statistical errors of measuring Na with the small probes.

Muscles Incubated in Hypertonic Solutions

The compartmentalization of extracellular solutes was clearly demonstrable after incubation in hypertonic solutions, in contrast to the observations made on normal resting muscle. The compartments containing much higher than cytoplasmic concentrations of extracellular solutes (e.g., Cl) included both broken and unbroken vacuoles. The size of the broken vacuoles (holes), however, may not have been representative of the in vivo state of these swollen structures. These regions, because of their high water content, could form preferred sites of ice crystal formation, and also have a greater tendency to break apart during sectioning, drying, or when exposed to the beam in the electron microscope. The precise identification of the swollen membrane system constituting the compartment (broken and unbroken vacuoles) containing high concentrations of extracellular solutes must await techniques that provide better contrast and detail than are available in the majority of unfixed, frozen-dried and vapor-stained cryo sections. Thus, although the location of the vacuoles adjacent to the Z line and their frequently paired disposition and apparent continuity with the longitudinal SR led to their identification as swollen terminal cisternae in a preliminary report (87), an alternate interpretation of the identity of the swollen compartments is possible (unpublished observations in collaboration with Clara Franzini-Armstrong; see note added in proof). We did not find in cryo sections the swelling of the longitudinal tubules of the SR previously observed in acrolein-fixed samples of muscles treated with hypertonic solutions (15). The location of the vacuoles in frequent pairs along the Z line ob-

served in the present study differed from the distribution and size (up to 10 μm) of the vacuoles observed in muscles fixed during stimulated efflux of permeant ions and nonelectrolytes (62).

The presence of high NaCl or sucrose or S (the latter in isethionate-treated muscles) in the swollen structures suggested that the extracellular solutes entered the vacuoles through diffusion from the extracellular space, rather than by active transport from the cytoplasm. Thus, while an active pump system could have been responsible for the entry of NaCl into such structures, neither sucrose (17) nor isethionate enters the cytoplasm and there is no evidence for an active transport system for either of these two solutes. The existence of this "extracellular" compartment is in agreement with the osmotic volume behavior (17, 31) and the possible increase in membrane capacity (95) of muscle in hypertonic solutions. The presence of this compartment, regardless of its identity, may have some bearing on the interpretation of physiological experiments in which hypertonic solutions are used to immobilize muscles during voltage clamp studies of charge movements (3, 81) and during the measurement of birefringence (9) and voltage-sensitive dye responses (12) considered to reflect the electrical behavior of the T-SR system.

Electron probe analysis of the cytoplasm (between vacuoles) of muscles treated with hypertonic solutions showed normal K concentrations, in agreement with earlier bulk chemical measurements of hypertonically treated muscle (14). The Cl content of the cytoplasm in these muscles was also normal, while electron probe analysis of averaged regions, including both the vacuoles and myofibrillar regions, showed an increased Cl content.

The presence of Ca granules in the longitudinal tubules of the SR of muscles treated with hypertonic solutions provides direct evidence of translocation of Ca by hypertonicity into the longitudinal tubular system. The initial release of Ca, presumably from the terminal cisternae, by hypertonic solutions has also been suggested on the basis of the transient contracture (14, 51, 52, 63) and the increase in aequorin signal (94) produced by hypertonicity. Total fiber Ca is not increased, and may be slightly decreased, by hypertonic solutions (14, 51), and the increase in the slow component of the exchangeable ^{45}Ca has been interpreted as being due to translocation of Ca into a less readily mobilizable compartment (51). The association of Mg (and P) with Ca in the granules found in the longitudinal SR may be related to the Mg requirement of the Ca ATPase of the SR and/or the proposed Mg-Ca exchange during Ca transport (56).

Finally, we wish to reemphasize that quantitative electron probe analysis combined with cryoultramicrotomy is a uniquely suitable technique for providing detailed information about the intracellular and transcellular distribution and movement of a variety of elements.

The excellent technical assistance of Mr. John Silcox is gratefully acknowledged. We thank Dr. Clara Franzini-Armstrong and Dr. Lee Peachey for valuable discussions.

Supported by HL-15835 to the Pennsylvania Muscle Institute and GM 00092.

This work was submitted to the graduate school of the University of Pennsylvania by A. V. Somlyo in partial fulfillment of the requirements for the degree of Doctor of Philosophy in Physiology.

Received for publication 12 November 1976, and in revised form 13 April 1977.

Note Added in Proof: Electron probe analysis of toadfish swimbladder striated muscle with improved count statistics for Na shows that neither Na nor Cl are compartmentalized in the SR (A. V. Somlyo, H. Shuman, and A. P. Somlyo. *Nature* [*Lond.*]. In press). In addition, recent studies on freeze-substituted frog muscles treated with hypertonic solutions show that the vacuoles containing extracellular solutes described in the present study are part of the T-tubular system (C. Franzini-Armstrong, A. V. Somlyo, J. Haeuser, T. Reese, and A. P. Somlyo. Manuscript in preparation).

REFERENCES

1. ADRIAN, R. H. 1956. The effect of internal and external potassium concentration on the membrane potential of frog muscle. *J. Physiol.* (*Lond.*). **133**:631–658.
2. ADRIAN, R. H. 1961. Internal chloride concentration and chloride efflux of frog muscle. *J. Physiol.* (*Lond.*). **156**:623–632.
3. ALMERS, W. 1975. Observations on intramembrane charge movements in skeletal muscle. *Philos. Trans. R. Soc. Lond. B. Biol. Sci.* **270**:507–513.
4. APPLETON, T. C. 1972. 'Dry' ultrathin frozen sections for electron microscopy and x-ray microanalysis: the cryostat approach. *Micron.* **3**:101–105.
5. APPLETON, T. C. 1974. A cryostat approach to ultrathin 'dry' frozen sections for electron microscopy: a morphological and x-ray analytical study. *J. Micros.* **100**:49–74.
6. ARMSTRONG, W. McD., and C. O. LEE. 1971. Sodium and potassium activities in normal and "so-

dium-rich" frog skeletal muscle. *Science (Wash. D. C.).* **171:**413–415.

7. ARMSTRONG, W. McD., W. WOJTKOWSKI, and W R. BIXENMAN. 1977. A new solid state microelectrode for measuring intracellular chloride activities. *Biochim. Biophys. Acta.* **465:**165–170.
8. BÁRÁNY, M., and K. BÁRÁNY. 1973. A proposal for the mechanism on contraction in intact frog muscle. *Cold Spring Harbor Symp. Quant. Biol.* **37:**157–167.
9. BAYLOR, S. M., and H. OETLIKER. 1975. Birefringence experiments on isolated skeletal muscle fibres suggest a possible signal from the sarcoplasmic reticulum. *Nature (Lond.).* **253:**97–101.
10. BERNHARD, W. 1971. Improved techniques for the preparation of ultrathin frozen sections. *J. Cell Biol.* **49:**731–746.
11. BEVINGTON, P. R. 1969. Data Reduction and Error Analysis for the Physical Sciences. McGraw-Hill Book Co., New York. 66–91.
12. BEZANILLA, F., and P. HOROWICZ. 1975. Fluorescence intensity changes associated with contractile activation in frog muscle stained with nile blue. *Am. J. Physiol.* **246:**709–735.
13. BIANCHI, C. P. 1968. Calcium in cells. Cell Calcium. Butterworth & Co. Ltd., London. 14–27.
14. BIANCHI, C. P., and T. C. BOLTON. 1974. Effect of hypertonic solutions and "glycerol treatment" on calcium and magnesium movements of frog skeletal muscle. *J. Pharmacol. Exp. Ther.* **188:**536–552.
15. BIRKS, R. I., and D. F. DAVEY. 1969. Osmotic responses demonstrating the extracellular character of the sarcoplasmic reticulum. *J. Physiol. (Lond.).* **202:**171–188.
16. BIRKS, R. I., and D. F. DAVEY. 1972. An analysis of volume changes in the T-tubes of frog skeletal muscle exposed to sucrose. *J. Physiol. (Lond.).* **222:**95–111.
17. BLINKS, J. R. 1965. Influence of osmotic strength on cross section and volume of isolated single muscle fibers. *J. Physiol. (Lond.).* **177:**42–47.
18. BOYLE, P. J., and E. J. CONWAY. 1941. Potassium accumulation in muscle and associated changes. *J. Physiol. (Lond.).* **100:**1–63.
19. BULLIVANT, S. 1970. Present status of freezing techniques. *In* Some Biological Techniques In Electron Microscopy. D. F. Parsons, editor. Academic Press, Inc., New York. 101–139.
20. BURT, C. T., T. GLONEK, and M. BÁRÁNY. 1976. Analysis of phosphate metabolites, the intracellular pH, and the state of adenosine triphosphate in intact muscle by phosphorus nuclear magnetic resonance. *J. Biol. Chem.* **251:**2584–2591.
21. CARVALHO, A. P., and B. LEO. 1967. Effects of ATP on the interaction of Ca, Mg and K with fragmented sarcoplasmic reticulum isolated from rabbit skeletal muscle. *J. Gen. Physiol.* **50:**1327–1352.
22. CASTEELS, R. 1971. The distribution of chloride ions in the smooth muscle cells of the guinea-pig's taenia coli. *J. Physiol. (Lond.).* **214:**225–243.
23. CHRISTENSEN, A. K. 1971. Frozen thin sections of fresh tissue for electron microscopy, with a description of pancreas and liver. *J. Cell Biol.* **51:**772–804.
24. COLEMAN, J. R., J. R. NILSSON, R. R. WARNER, and P. BATT. 1973. Electron probe analysis of refractive bodies in *Amoeba proteus*. *Exp. Cell. Res.* **76:**31–40.
25. COLEMAN, J. R., and A. R. TEREPKA. 1972. Electron probe analysis of the calcium distribution in cells of the embryonic chick chorioallantoic membrane. I. A critical evaluation of techniques. *J. Histochem. Cytochem.* **20:**401–413.
26. COLEMAN, J. R., and A. R. TEREPKA. 1972. Electron probe analysis of the calcium distribution in cells of the embryonic chick chorioallantoic membrane. II. Demonstration of intracellular location during active transcellular transport. *J. Histochem. Cytochem.* **20:**414–424.
27. CONWAY, E. J. 1957. Nature and significance of concentration relations of potassium and sodium ions in skeletal muscle. *Physiol. Rev.* **37:**84–132.
28. COSTANTIN, L. L. 1975. Contractile activation in skeletal muscle. *Prog. Biophys. Mol. Biol.* **29:**197–224.
29. DORGE, A., K. GEHRING, W. NAGEL, and K. THURAU. 1974. Intracellular Na-K concentration of frog skin at different states of Na transport. *In* Microprobe Analysis as Applied to Cells and Tissues. T. Hall, P. Echlin, and R. Kaufmann, editors. Academic Press, Inc., New York. 337–349.
30. DOTY, S. B., C. W. LEE, and W. G. BANFIELD. 1974. A method for obtaining ultrathin frozen sections from fresh or glutaraldehyde-fixed tissues. *Histochem. J.* **6:**383–393.
31. DYDYNSKA, M., and D. R. WILKIE. 1963. The osmotic properties of striated muscle fibers in hypertonic solutions. *J. Physiol. (Lond.)* **169:**312–329.
32. EBASHI, S., and M. ENDO. 1968. Calcium ion and muscle contraction. *In* Progress in Biophysics and Molecular Biology. J. A. V. Butler and D. Noble, editors. Pergamon Press, New York. 123–183.
33. EISENBERG, R. S., and P. W. GAGE. 1969. Ionic conductances of the surface and transverse tubular membranes of frog sartorius fibers. *J. Gen. Physiol.* **53:**279–297.
34. ENDO, M. 1966. Entry of fluorescent dyes into the sarcotubular system of the frog muscle. *J. Physiol. (Lond.).* **185:**224–238.
35. ENDO, M. 1975. Mechanism of action of caffeine on the sarcoplasmic reticulum of skeletal muscle. *Proc. Jpn. Acad.* **51:**479–484.
36. FALK, G., and P. FATT. 1964. Linear electrical properties of striated muscle fibers observed with intracellular electrodes. *Proc. R. Soc. Lond. B.*

Biol. Sci. **160**:69–123.

37. FORD, L. E., and R. J. PODOLSKY. 1972. Intracellular calcium movements in skinned muscle fibers. *J. Physiol. (Lond.)* **223**:21–33.
38. FRANZINI-ARMSTRONG, C. 1970. Studies of the triad. I. Structure of the junction in frog twitch fibers. *J. Cell Biol.* **47**:488–499.
39. FRANZINI-ARMSTRONG, C. 1974. Freeze fracture of skeletal muscle from the tarantula spider. Structural differentiations of sarcoplasmic reticulum and transverse tubular system membranes. *J. Cell Biol.* **61**:501–513.
40. FRANZINI-ARMSTRONG, C. 1975. Membrane particles and transmission at the triad. *Fed. Proc.* **34**:1382–1389.
41. GARFIELD, R. E., and A. P. SOMLYO. 1975. Electron probe analysis and ultrastructure of cultured, freeze-dried vascular smooth muscle. Proceedings of the 33rd Annual EMSA Meetings. 558.
42. GERSH, I., and J. L. STEPHENSON. 1954. Freezing and drying of tissues for morphological and histochemical studies. *In* Biological Applications of Freezing and Drying. R. J. C. Harris, editor. Academic Press, Inc., New York. 329–384.
43. GILBERT, D. L., and J. MCGANN. 1960. Magnesium equilibrium in muscle. *J. Gen. Physiol.* **43**:1103.
44. GUPTA, B. L., T. A. HALL, S. H. P. MADDRELL, and R. B. MORETON. 1976. Distribution of ions in a fluid-transporting epithelium determined by electron-probe x-ray microanalysis. *Nature (Lond.).* **264**:284–287.
45. HALL, T. A. 1971. The microprobe assay of chemical elements. *In* Physical Techniques in Biological Research. Vol. IA. G. Oster, editor. Academic Press, Inc. New York.
46. HARRIS, E. J. 1963. Distribution and movement of muscle chloride. *J. Physiol. (Lond.).* **166**:87–109.
47. HODGKIN, A. L., and P. HOROWICZ. 1959. Movements of Na and K in single muscle fibers. *J. Physiol. (Lond.).* **145**:405–432.
48. HODGKIN, A. L., and P. HOROWICZ. 1959. The influence of potassium and chloride ions on the membrane potential of single muscle fibers. *J. Physiol. (Lond.).* **148**:127–160.
49. HODGKIN, A. L., and P. HOROWICZ. 1960. The effect of sudden changes in ionic concentrations on the membrane potential of single muscle fibers. *J. Physiol. (Lond.).* **153**:370–385.
50. HODGKIN, A. L., and S. NAKAJIMA. 1972. Analysis of the membrane capacity in frog muscle. *J. Physiol. (Lond.).* **221**:121–136.
51. HOMSHER, E., F. BRIGGS, and R. M. WISE. 1974. Effects of hypertonicity on resting and contracting frog skeletal muscles. *Am. J. Physiol.* **226**:855–863.
52. HOWARTH, J. V. 1958. The behavior of frog muscle in hypertonic solution. *J. Physiol. (Lond.).* **144**:167–175.
53. HUXLEY, H. E., S. PAGE, and D. R. WILKIE. 1963. An electron microscopic study of muscle in hypertonic solutions. Appendix to M. Dydynska and D. R. Wilkie. *J. Physiol. (Lond.).* **169**:312–329.
54. INGRAM, D. F., M. J. INGRAM, and C. A. M. HOGBEN. 1974. An analysis of the freeze-dried, plastic-embedded electron probe specimen preparation. *In* Microprobe Analysis as Applied to Cells and Tissues. T. Hall, P. Echlin, and R. Kaufmann, Academic Press, Inc., New York. 119–145.
55. JONES, A. W., A. P. SOMLYO, and A. V. SOMLYO. 1973. Potassium accumulation in smooth muscle and associated ultrastructural changes. *J. Physiol. (Lond.).* **232**:247.
56. KANAZAWA, T., S. YAMADA, T. YAMAMOTO, and Y. TONOMURA. 1971. Reaction mechanism of the Ca^{2+}-dependent ATPase of sarcoplasmic reticulum from skeletal muscle. *J. Biochem.* **70**:95–123.
57. KAO, C. Y., and A. NISHIYAMA. 1964. Ovarian hormones and resting potential of rabbit uterine smooth muscle. *Am. J. Physiol.* **207**:793–799.
58. KERNAN, R. P., M. MACDERMOTT, and W. WESTPHAL. 1974. Measurement of chloride activity within frog sartorius muscle fibres by means of chloride-sensitive micro-electrodes. *J. Physiol. (Lond.).* **241**:60–61P.
59. KEYNES, R. D. 1963. Chloride in the squad giant axon. *J. Physiol. (Lond.).* **169**:690–705.
60. KEYNES, R. D., and R. A. STEINHARDT. 1968. The components of the sodium efflux in frog muscle. *J. Physiol. (Lond.).* **198**:581–599.
61. KOSTYUK, P. G., Z. A. SOROKINA, and YU D. KHOLODOVA. 1969. Measurements of activity of hydrogen, potassium and sodium ions in striated muscle fibers and nerve cells. *In* Glass Microelectrodes. M. Lavallée, O. F. Schanne, and N. C. Hébert, editors. J. Wiley and Sons, Inc., New York. 322–338.
62. KROLENKO, S. A. 1973. Vacuolation of skeletal muscle fibers. VI. The origination of vacuoles during efflux of sugars and mineral ions. *Tsitologiya.* **15**(10):1244–1247.
63. LÄNNERGREN, J., and J. NOTH. 1973. Tension in isolated frog muscle fibers induced by hypertonic solutions. *J. Gen. Physiol.* **61**:158–175.
64. LECHENE, C. 1975. Applications of electron probe microanalysis in physiology. Proceedings of the 10th Annual Conference of the Microbeam Analysis Society. 40A–40G.
65. LECHENE, C., T. STRUNK, R. WARNER, and C. CONTY. 1975. Perspectives in electron probe microanalysis of biological samples kept frozen. Proceedings of the 10th Annual Conference of the Microbeam Analysis Society. 49A–49E.
66. LEE, C. O., and W. MCD. ARMSTRONG. 1974. State and distribution of potassium and sodium ions in frog skeletal muscle. *J. Membr. Biol.* **15**:331–362.
67. LEV, A. A. 1964. Determination of activity and

activity coefficients of potassium and sodium ions in frog muscle fibres. *Nature (Lond.)*. **201:**1132–1134.

68. MacLennan, D. H., and P. C. Holland. 1975. Calcium transport in sarcoplasmic reticulum. *Ann. Rev. Biophys. Bioeng.* **4:**377–404.
69. Makino, H., and E. Page. 1975. Net movements of Na, Li and Cl between sarcotubules and extracellular space in rat ventricles. *Fed. Proc.* **34:**413.
70. Mobley, B. A., and B. R. Eisenberg. 1975. Sizes of components in frog skeletal muscle measured by methods of stereology. *J. Gen. Physiol.* **66:**31–45.
71. Moor, H. 1971. Recent progress in the freeze-etching technique. *Phil. Trans. R. Soc. Lond. B. Biol. Sci.* **261:**121.
72. Nichols, B. L., H. A. Soriano, D. S. Sachen, L. Burns, C. F. Hazelwood, and S. L. Kimzey. 1974. Electron probe localization of electrolytes in immature muscle. *Johns Hopkins Med. J.* 322–335.
73. Page, E., and P. Polimeni. 1972. Magnesium exchange in rat ventricle. *J. Physiol. (Lond.)*. **224:**121–139.
74. Peachey, L. D. 1965. The sarcoplasmic reticulum and transverse tubules of the frog's sartorius. *J. Cell Biol.* **2:**209–231.
75. Peachey, L. D., and R. H. Adrian. 1973. Electrical properties of the transverse tubular system. *In* The Structure and Function of Muscle. Vol. 3. Ed. G. H. Bourne. Academic Press, Inc., New York. 1–29.
76. Podolsky, R. J., T. Hall, and S. L. Hatchett. 1970. Identification of oxalate precipitates in striated muscle fibers. *J. Cell Biol.* **44:**699–702.
77. Riehle, W. 1968. Ueber die Vitrifizierung verdünnter wässriger Lösungen. Ph.D. Thesis. Juris Druck and Verlag, Zürich.
78. Robards, A. W. 1974. Ultrastructural methods for looking at frozen cells. *Sci. Prog.* **61:**1–40.
79. Rogus, E., and K. L. Zierler. 1973. Sodium and water contents of sarcoplasm and sarcoplasmic reticulum in rat skeletal muscle: effects of anisotonic media, ouabain and external sodium. *J. Physiol. (Lond.)*. **233:**227–270.
80. Russell, J. M. 1976. ATP-dependent chloride influx into internally dialyzed squid giant axons. *J. Membr. Biol.* **28:**335–349.
81. Schneider, M. F., and W. K. Chandler. 1973. Voltage dependent charge movement in skeletal muscle: a possible step in excitation-contraction coupling. *Nature (Lond.)*. **242:**244–246.
82. Shuman, H., and A. P. Somlyo. 1976. Electron probe x-ray analysis of single ferritin molecules. *Proc. Natl. Acad. Sci. U. S. A.* **73:**1193–1195.
83. Shuman, H., A. V. Somlyo, and A. P. Somlyo. 1976. Quantitative electron probe microanalysis of biological thin sections: methods and validity. *Ultramicros.* **1:**317–339.
84. Shuman, H., A. V. Somlyo, and A. P. Somlyo. 1977. Theoretical and practical limits of ed x-ray analysis of biological thin sections. *Scan. Elec. Miscros.* **1:**663–672.
85. Sjodin, R. A., and L. A. Beaugé. 1973. An analysis of the leakages of sodium ions into and potassium ions out of striated muscle cells. *J. Gen. Physiol.* **61:**222–250.
86. Sjöström, M., and L. E. Thornell. 1975. Preparing sections of skeletal muscle for transmission electron analytical microscopy (TEAM) of diffusible elements. *J. Microsc.* **103:**1–12.
87. Somlyo, A. V., H. Shuman, and A. P. Somlyo. 1976. Chloride compartmentalization in striated muscle: quantitative electron probe analysis. *J. Cell Biol.* **70(2,** Pt. 2):336 a. (Abstr.).
88. Somlyo, A. V., H. Shuman and A. P. Somlyo. 1976. Electron probe analysis of vertebrate smooth muscle: distribution of Ca and Cl. Proceedings of the 34th Annual EMSA Meeting. 334.
89. Somlyo, A. V., H. Shuman and A. P. Somlyo. 1977. Intracellular $[Cl]_i$ in muscle: quantitative electron probe analysis of cryo sections. *Biophysical J.* **17:**7 a. (Abstr.).
90. Somlyo, A. V., J. Silcox and A. P. Somlyo. 1975. Electron probe analysis and cryoultramicrotomy of cardiac muscle: mitochondrial granules. Proc. 33rd Ann. EMSA Meetings. 532.
91. Somlyo, A. P., A. V. Somlyo, C. E. Devine, P. D. Peters, and T. A. Hall. 1974. Electron microscopy and electron probe analysis of mitochondrial cation accumulation in smooth muscle. *J. Cell Biol.* **61:**723–742.
92. Spector, W. S. 1961. Handbook of Biological Data. W. B. Saunders Co, Philadelphia. 72.
93. Strickholm, A., and B. G. Wallin. 1965. Intracellular chloride activity of crayfish giant axons. *Nature (Lond.)*. **208:**790–791.
94. Taylor, S. R., R. Rüdel, and J. R. Blinks. 1975. Calcium transients in amphibian muscle. *Fed. Proc.* **34:**1379–1381.
95. Valdiosera, R., C. Clausen, and R. S. Eisenberg. 1974. Impedance of frog skeletal muscle fibers in various solutions. *J. Gen. Physiol.* **63:**460–491.
96. Villegas, J., L. Villegas, and R. Villegas. 1965. Sodium, potassium, and chloride concentration in the Schwann cell and axon of the squid nerve fiber. *J. Gen. Physiol.* **49:**1–7.
97. Weiner, M. W. 1975. Mitochondrial permeability to chloride ion. *Am. J. Physiol.* **228:**122–126.
98. Winegrad, S. 1968. Intracellular calcium movements in frog skeletal muscle during recovery from tetanus. *J. Gen. Physiol.* **51:**65–83.
99. Winegrad, S. 1970. The intracellular site of calcium activation of contraction in frog skeletal muscle. *J. Gen. Physiol.* **55:**77–88.